AD-A178 466 RADIATION HARDENED SILICA-BASED OPTICAL FIBERS(U) GTE 1/1
LABS INC WALTHAM MA W J MINISCALCO ET AL. OCT 86
RADC-TR-86-181 F19628-85-C-0050

UNCLASSIFIED F/G 20/6 NL

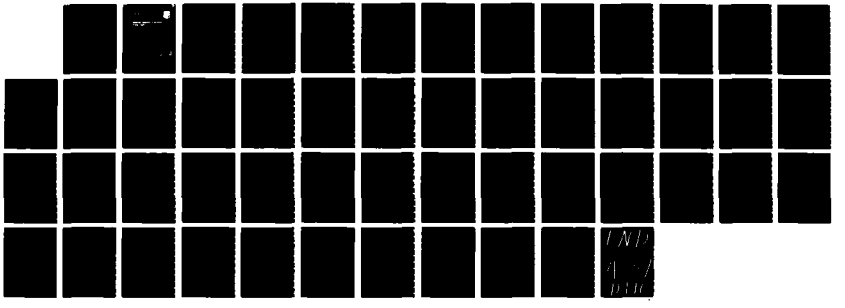

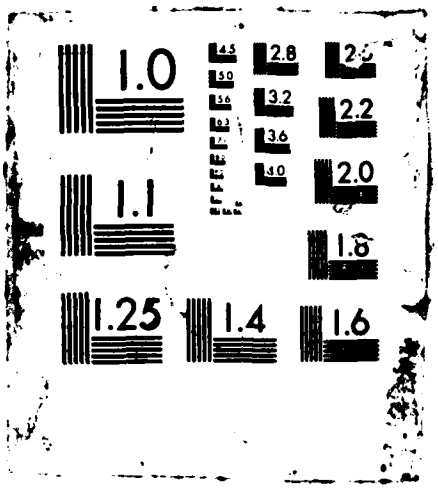
1.0
1.1
1.25
1.4
1.6
2.8
3.2
3.6
4.0
2.2
2.0
1.8

(12)

RADC-TR-86-181
Interim Report
October 1986

RADIATION HARDENED SILICA-BASED OPTICAL FIBERS

GTE Laboratories Incorporated

W. J. Miniscalco, T. Wei and P. I. K. Onorato

ROME AIR DEVELOPMENT CENTER
Air Force Systems Command
Griffiss Air Force Base, NY 13441-5700

RADC TR-86-181 has been reviewed and approved for publication.

This report has been reviewed by the RADC Public Affairs Office (PA) and is releasable to the National Technical Information Service (NTIS). At NTIS it will be releasable to the general public, including foreign nations.

APPROVED:

James A. Wall

JAMES WALL
Project Engineer

APPROVED:

Harold Roth

HAROLD ROTH
Director of Solid State Sciences

FOR THE COMMANDER:

John A. Ritz

JOHN A. RITZ
Directorate of Plans and Programs

If your address has changed or if you wish to be removed from the RADC mailing list, or if the addressee is no longer employed by your organization, please notify RADC (ESR) Hanscom AFB MA 01731-5000. This will assist us in maintaining a current mailing list.

Do not return copies of this report unless contractual obligations or notices on a specific document requires that it be returned.

UNCLASSIFIED
SECURITY CLASSIFICATION OF THIS PAGE

ADA178466

REPORT DOCUMENTATION PAGE

1a. REPORT SECURITY CLASSIFICATION UNCLASSIFIED	1b. RESTRICTIVE MARKINGS N/A
2a. SECURITY CLASSIFICATION AUTHORITY N/A	3. DISTRIBUTION / AVAILABILITY OF REPORT Approved for public release; distribution unlimited.
2b. DECLASSIFICATION / DOWNGRADING SCHEDULE N/A	
4. PERFORMING ORGANIZATION REPORT NUMBER(S) N/A	5. MONITORING ORGANIZATION REPORT NUMBER(S) RADC-TR-86-181
6a. NAME OF PERFORMING ORGANIZATION GTE Laboratories Inc. — 6b. OFFICE SYMBOL (If applicable)	7a. NAME OF MONITORING ORGANIZATION Rome Air Development Center (ESR)
6c. ADDRESS (City, State, and ZIP Code) 40 Sylvan Road Waltham MA 02254	7b. ADDRESS (City, State, and ZIP Code) Hanscom AFB MA 01731-5000
8a. NAME OF FUNDING / SPONSORING ORGANIZATION Rome Air Development Center — 8b. OFFICE SYMBOL (If applicable) ESR	9. PROCUREMENT INSTRUMENT IDENTIFICATION NUMBER F19628-85-C-0050
8c. ADDRESS (City, State, and ZIP Code) Hanscom AFB MA 01731-5000	10 SOURCE OF FUNDING NUMBERS PROGRAM ELEMENT NO. 62702F — PROJECT NO. 4600 — TASK NO. 20 — WORK UNIT ACCESSION NO. 47

11. TITLE (Include Security Classification)

RADIATION HARDENED SILICA-BASED OPTICAL FIBERS

12. PERSONAL AUTHOR(S)
W.J. Miniscalco, T. Wei, and P.I.K. Onorato

13a. TYPE OF REPORT	13b. TIME COVERED	14. DATE OF REPORT (Year, Month, Day)	15. PAGE COUNT
Interim	FROM Mar 85 TO Mar 86	October 1986	54

16. SUPPLEMENTARY NOTATION
N/A

17. COSATI CODES			18. SUBJECT TERMS (Continue on reverse if necessary and identify by block number)
FIELD	GROUP	SUB-GROUP	
20	12		Optical Fibers, Radiation Effects, and Glass Structure

19. ABSTRACT (Continue on reverse if necessary and identify by block number)

For the defect passivation approach, we have completed the evaluation of the effects of hydrogen treatment. Considerable reduction in radiation-induced absorption at long wavelengths ($\lambda > 1\ \mu m$) has been observed for hydrogen-treated fibers. Posttreatment of irradiated fibers by hydrogen also increases the hardness of the fibers under subsequent irradiation. In addition, we found photoluminescence to be an effective characterization tool which provides additional evidence for the passivating effect of hydrogen treatment.

20. DISTRIBUTION / AVAILABILITY OF ABSTRACT ☐ UNCLASSIFIED/UNLIMITED ☑ SAME AS RPT ☐ DTIC USERS	21 ABSTRACT SECURITY CLASSIFICATION UNCLASSIFIED
22a. NAME OF RESPONSIBLE INDIVIDUAL JAMES A. WALL	22b. TELEPHONE (Include Area Code) (617)377-4031 — 22c. OFFICE SYMBOL RADC (ESR)

DD FORM 1473, 84 MAR — 83 APR edition may be used until exhausted. All other editions are obsolete.

SECURITY CLASSIFICATION OF THIS PAGE
UNCLASSIFIED

CONTENTS

1. INTRODUCTION AND SUMMARY

1.1 OBJECTIVE

The objective of this program is to determine what influences the sensitivity of optical fiber to radiation and use this knowledge to develop fiber with improved radiation resistance. The effort is directed toward graded index fibers which are required for high bandwidth applications. Because of the dopants in the core which are required to grade the refractive index, these fibers are much more sensitive to radiation-induced loss than the lower bandwidth pure-silica-core fibers.

The program is based upon the well established concept that radiation-induced absorption is governed by pre-existing defects in the glass. The induced loss is due to color centers which form when existing defects trap the electrons and holes generated by ionizing radiation. The emphasis is on obtaining a fundamental understanding of the relationship between defects in the as-drawn fiber and the glass composition and processing conditio s. Using this knowledge, fibers with parameters predicted to be favorable will be fabricated and tested. For the most radiation-resistant optical fibers developed, complete documentation on compositions and fabrication processes will be provided in sufficient detail to allow transfer to a manufacturing unit.

1.2 APPROACH

Induced absorption occurs when existing defects in the glass form color centers by trapping electrons and holes generated by ionizing radiation. Three technical approaches are being pursued which are based upon the principle of reducing the concentrations of these defects or mitigating their effect.

I. Defect Passivation

One method to prevent defects in as-drawn fiber from capturing carriers and forming color centers is to transform them into benign defects. The latter are defined as either defects which form color centers that absorb outside the wavelength range of interest, or, preferably, ones without the ability to capture an electron or hole.

II. Defect Minimization

Reducing the concentration of defects in the as-drawn fiber will reduce the amount of color center absorption following irradiation. Common sources of defects are dopants, mechanical stress, and thermomechanical stress.

III. · Recombination Centers

Many defects and impurities have localized electronic states located deep within the energy gap of the glass. These will serve as recombination centers if the states have the ability to trap both electrons and holes. These centers will reduce induced loss if they can compete successfully with other defects for the carriers generated by the radiation.

The program is divided into three phases. In the first or Exploratory Phase all of the three technical approaches will be pursued simultaneously. This phase has a duration of ≈15 months. The second or Refinement Phase

will last ≈10 months during which the activity will focus on only the most promising approach or combination of approaches. The final or Optimization Phase involves fine tuning of the successful approaches, including the exploration of tradeoffs. This report covers the first 12 months of the Exploratory Phase.

1.3 PROCEDURE

The program involves both an experimental and a theoretical effort. The former consists of carefully chosen experiments based upon established concepts from the physics of defects in glasses. The primary experimental tool is the measurement of radiation-induced loss in the fibers. This is being done both *in situ* at RADC at a fixed wavelength, and as post irradiation spectral measurements at GTE Laboratories. Differential modal attenuation is also being applied in some of the approaches. More selective techniques such as Raman scattering and photoluminescence are also being tried, and the latter method shows great promise for characterizing defects in fibers. These experimental methods are being supplemented with molecular dynamic simulations of the glass to determine defect types and concentrations. This involves computer generation of glass structures which are then analyzed to identify defects. The objective of the molecular dynamics simulations is to establish the correlation between structural defects and the dopants used either to modify the index of refraction or to introduce recombination centers.

1.4 SUMMARY OF RESULTS

All of the approaches investigated to date have been extremely effective at reducing induced loss. Fibers have already been produced which are comparable in radiation hardness to the best doped-core fibers reported in the

literature. No results are yet available for the recombination center approach, but combinations of at least the defect passivation and defect minimization approaches now appear to be extremely promising avenues to further improvements.

In the defect passivation approach, the major effort has been in the area of hydrogen treatment of fibers to convert existing defects into types which result in less attenuation when irradiated. This technique is showing great promise for hardening fibers. The first series of experiments were conducted on fibers with a Ge/P-codoped core. The fibers which had been treated with hydrogen prior to irradiation demonstrated significantly less induced loss. The effect was found to depend upon the extent of the reaction of hydrogen with the defects: treatment with a higher hydrogen partial pressure improved the hardness still further. It was also found that hydrogen treatment following irradiation significantly reduced the induced loss and made the fibers much harder in subsequent irradiations. Since phosphorus-doped fibers are very radiation sensitive, this technique will now be applied to much harder Ge/F-doped fibers discussed below.

An effort was made to find a characterization technique with greater selectivity than attenuation measurements for the identification of specific centers. Raman scattering and photoluminescence investigations of the fibers were undertaken, and although Raman scattering does not seem to be sensitive to the centers of interest, photoluminescence was found to be an effective tool. Significant differences were found among fibers subjected to differing treatments. In particular, the intensity of the luminescence band at 650 nm, attributed to drawing and/or radiation induced centers, was found to have an inverse correlation with loss. The luminescence intensity also increased with photobleaching. These results support our premise that there are a wide variety of defects present in fiber, some more deleterious than others in a radiation environment, and that defects can be converted from one type to another.

The defect minimization approach was the other area which was focused on in the current reporting period. The molecular dynamic simulations were successful in generating pure silica glass, pure germania glass, and a 10 mole% Ge-doped silica glass. The glass simulation is now well in hand and the emphasis has turned to the analysis programs, particularly the one which calculates the radial distribution functions and coordination numbers. This analysis is now being applied to the glasses to determine the types and concentrations of structural defects. The Ge-doped silica has been the most thoroughly analyzed glass, and no evidence was found for defects resulting from anomalous silicon-oxygen distances. More detailed analysis of these glasses will be required.

Important results have been obtained in the investigation of the role of drawing-induced defects in radiation sensitivity. Four fibers from the same preform were drawn under different conditions of temperature, speed, and tension. Clear evidence was found that a lower draw temperature produces harder fiber. No unambiguous correlation could be found for the effect of drawing speed. These fibers had a Ge/F-codoped core and a F-doped depressed cladding. The induced loss was quite low for all these fibers and was comparable to the best values reported for doped-core multimode fiber in the literature. The conditions for low drawing-induced defect concentrations established by this study are being applied in the other areas of the program.

The investigation of core/clad interfacial stress used differential modal analysis in addition to standard loss spectrum measurements. The DMA measurements revealed that prior to irradiation the higher modes suffered greater attenuation in the fibers with the highly stressed core/clad interface than in the low stress fibers. After irradiation the differences between the high and low stress fibers were found to be insignificant from both attenuation and DMA measurements. It was concluded that core/clad interfacial stress does not play a major role in determining the radiation sensitivity of a fiber since only the higher modes are affected and these modes do not propagate long distances under any circumstances.

Work has recently begun on improving radiation resistance by reducing the dopant concentration in the core. Since doping introduces defects into glass by altering the structure, we expect that induced loss can be reduced by lowering the dopant concentration or by using combinations of dopants which do not introduce defects. To this end, three preforms have been fabricated with different concentrations of germanium and fluorine in the core. The fibers have been drawn and are in the process of being tested.

2. DEFECT PASSIVATION

2.1 HYDROGEN TREATMENT

One method to prevent defects in as-drawn fiber from capturing carriers and forming color centers is to transform them into benign defects which do not absorb in the spectral region of interest. This approach has already been exploited in reducing radiation damage in bulk vitreous silica through the use of hydrothermal treatment [1]. The effect of water is to transform an E' defect and a nonbridging oxygen into two neutral silanol groups. Similar studies indicated that fibers with high hydroxyl content were less prone to damage at short wavelengths, although excessive hydroxyl absorption was observed at long wavelengths [2]. Recently there have been many studies on increases of optical attenuation in optical fibers due to hydrogen permeation [3]. This loss increase phenomenon is associated with the diffusion of hydrogen to the fiber core and subsequent chemical reactions with structural defects in the glass to form OH species and new defect centers. To test the applicability of hydrogen treatment in defect passivation, we have compared the radiation resistance of a treated fiber with that of an untreated length of the same fiber.

In the first experiment, we treated a 250-m-long section from a Ge/P-co-doped, graded-index optical fiber. This piece was placed in an atmosphere with a hydrogen partial pressure of 0.06 atm at 70°C for seven days. After the treatment, dissolved hydrogen was evacuated from the fiber. Figure 1 shows the change in loss spectrum after the hydrogen pretreatment. The hydroxyl concentration was found to have increased from 73 ppb to 115 ppb. The additional loss above 1.5 μm was due to the formation of POH. Portions of the hydrogen treated fiber and an untreated control fiber were irradiated

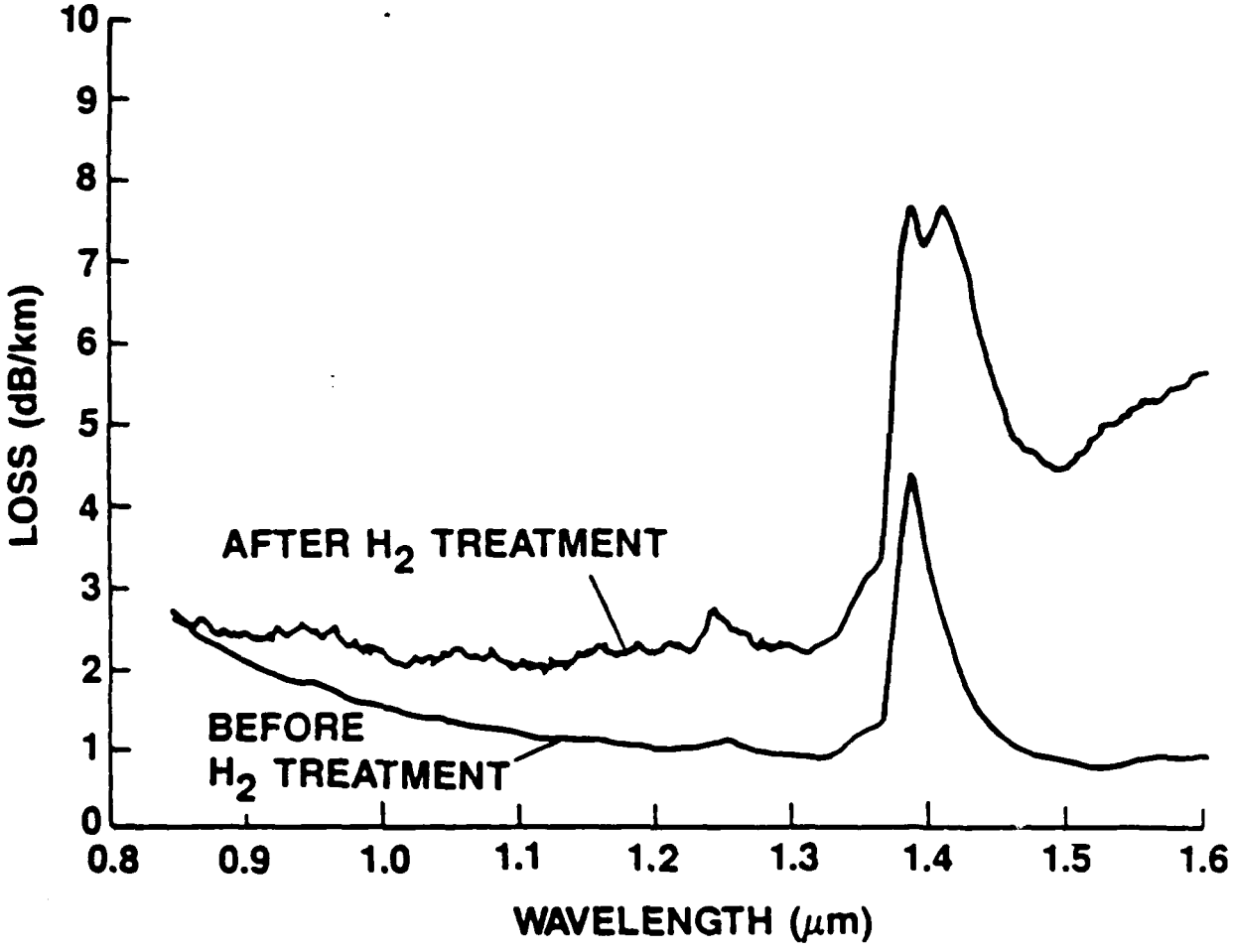

Figure 1

Loss spectra of fiber before and after hydrogen treatment (0.06 atm, 70°C, 7 days) showing the resultant increase in hydroxyl absorption.

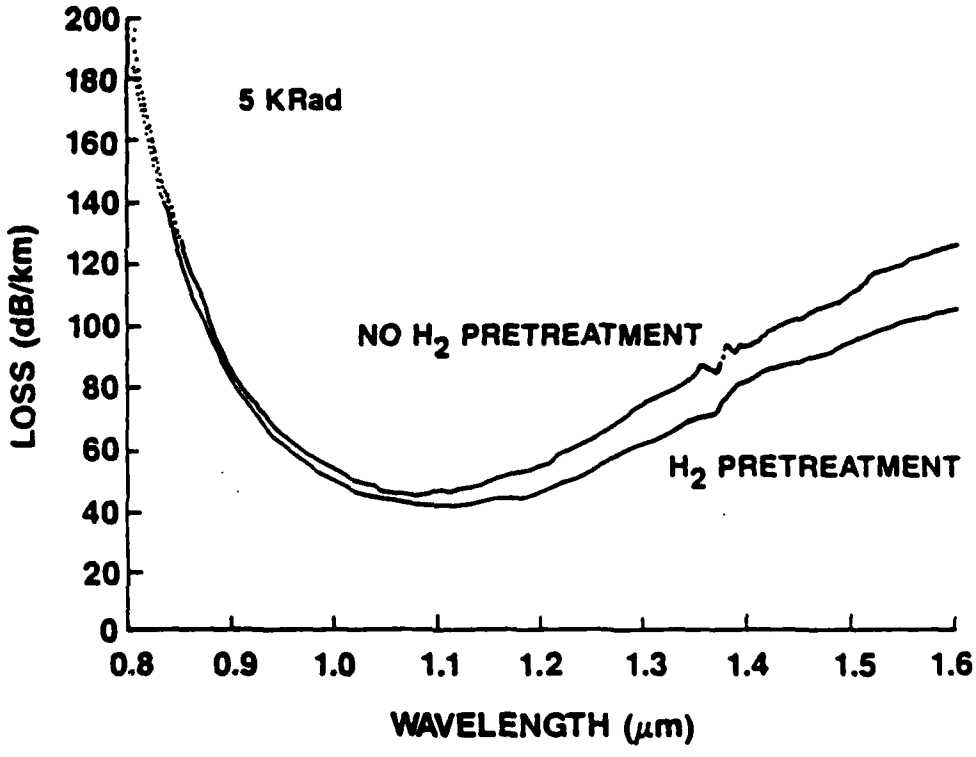

Figure 2

Loss spectra of fibers with and without hydrogen pretreatment (0.06 atm, 70°C, 7 days) after 5 kRad dose.

using the ^{60}Co source at RADC. The total dose was 5 kRad. Figure 2 shows the loss spectra from 800-1600 nm for the treated and untreated fibers after irradiation. The high loss at shorter wavelengths is expected for a phosphorus doped optical fiber. These measurements reveal a clear difference between the treated and untreated fibers which increases with increasing wavelength (Figure 2). The attenuation (dB/km) is ≈20% lower for the hydrogen-treated fiber at 1600 nm. This modest difference is not surprising, considering the low hydrogen partial pressure used in the pretreatment.

In the second experiment we treated fibers in an atmosphere with a hydrogen partial pressure of 0.86 atm at 65°C for seven days to observe effects of higher hydrogen partial pressure and hydrogen posttreatment on radiation-induced losses. Three samples were selected for the hydrogen treatment: both of the irradiated fibers from the first experiment and a piece of the as-drawn fiber. Figure 3 shows the loss spectra of the irradiated fibers after the hydrogen posttreatment. The data reveal a dramatic recovery in attenuation to 10-25 dB/km at 1100 nm and 20-30 dB/km at 850 nm. They also reveal the difference between the pretreated and untreated fibers when subjected to hydrogen posttreatment: the pretreated fiber has retained its overall lower attenuation. All treated fibers and a control sample were subjected to ≈5 kRad γ irradiation. Figure 4 compares the loss spectra after irradiation with and without the hydrogen treatment. We observe on the order of 50 dB/km less induced attenuation at long wavelengths ($\lambda > 1$ μm) for a hydrogen-treated fiber. This is significantly better than results from the first experiment and is attributed to the use of a higher hydrogen partial pressure. We also observed improvement in radiation hardness as a result of postirradiation hydrogen treatment. Posttreatment of irradiated fibers by hydrogen can significantly reduce existing radiation-induced absorption (see Figure 3) and increase the hardness of fibers under subsequent irradiation. Figure 5 shows the loss spectra after a second irradiation for posttreated fibers. Note that there is little difference between two posttreated fibers and the overall loss is lower than that shown in Figure 4. In all attenuation measurements, special care was taken to avoid the photobleaching effect observed with earlier samples.

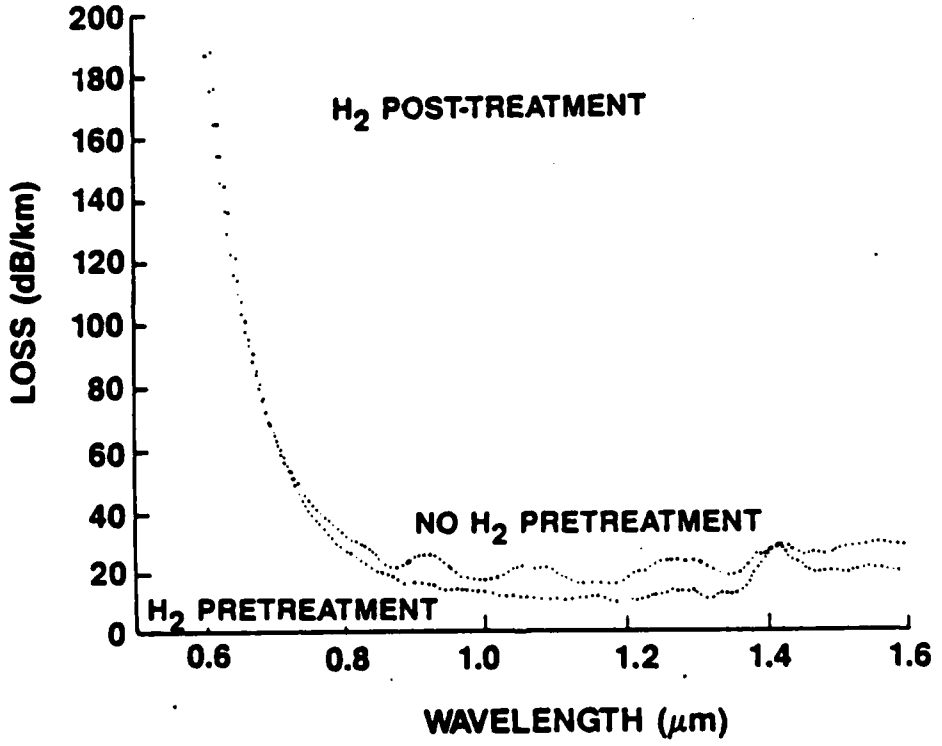

Figure 3

Loss spectra of fibers retreated (0.86 atm, 65°C, 7 days) after irradiation. Lower curve: with hydrogen pretreatment (0.06 atm, 70°C, 7 days). Upper curve: without hydrogen pretreatment.

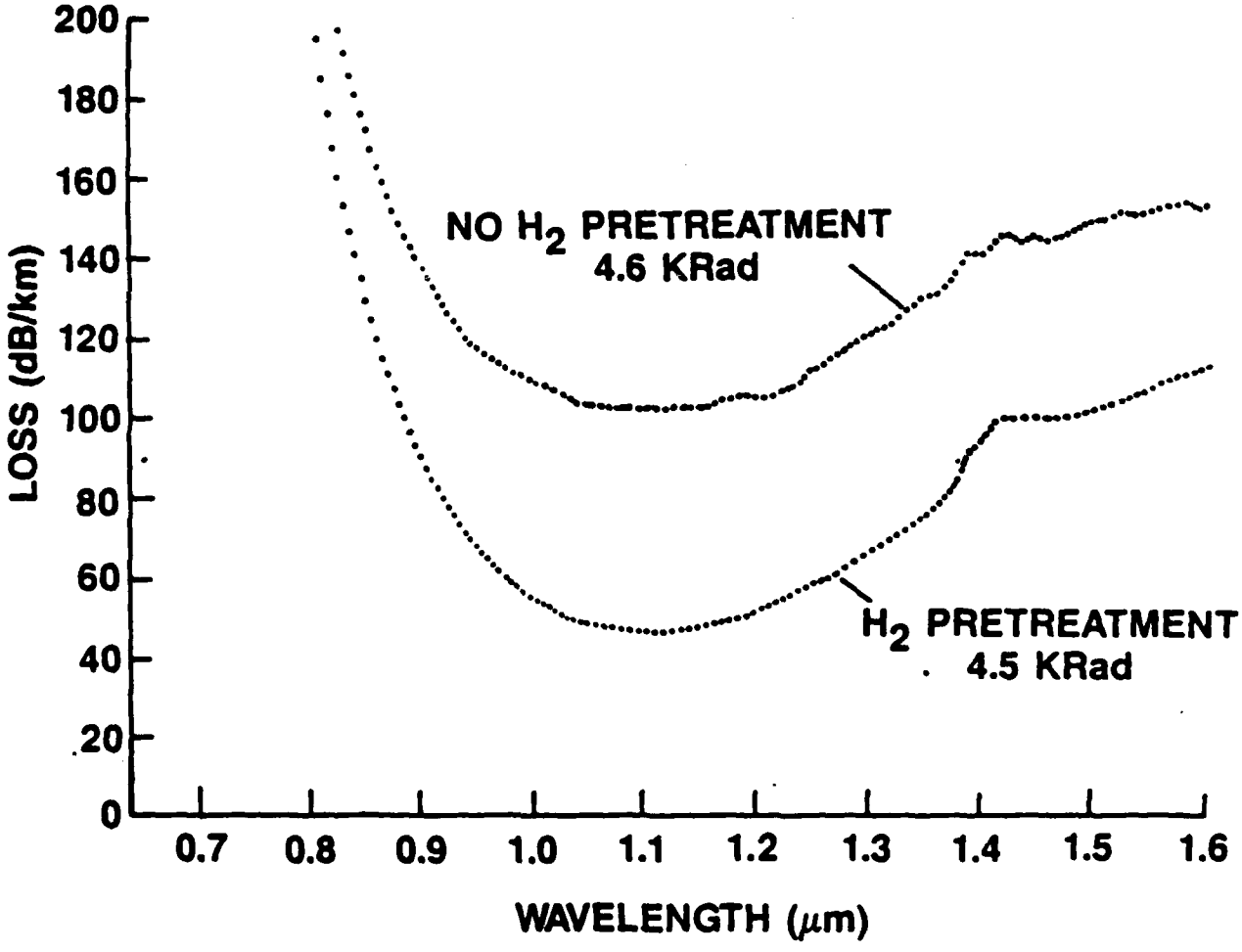

Figure 4

Loss spectra after 4.6 kRad dose for fibers with and without hydrogen pretreatment (0.86 atm, 65°C, 7 days).

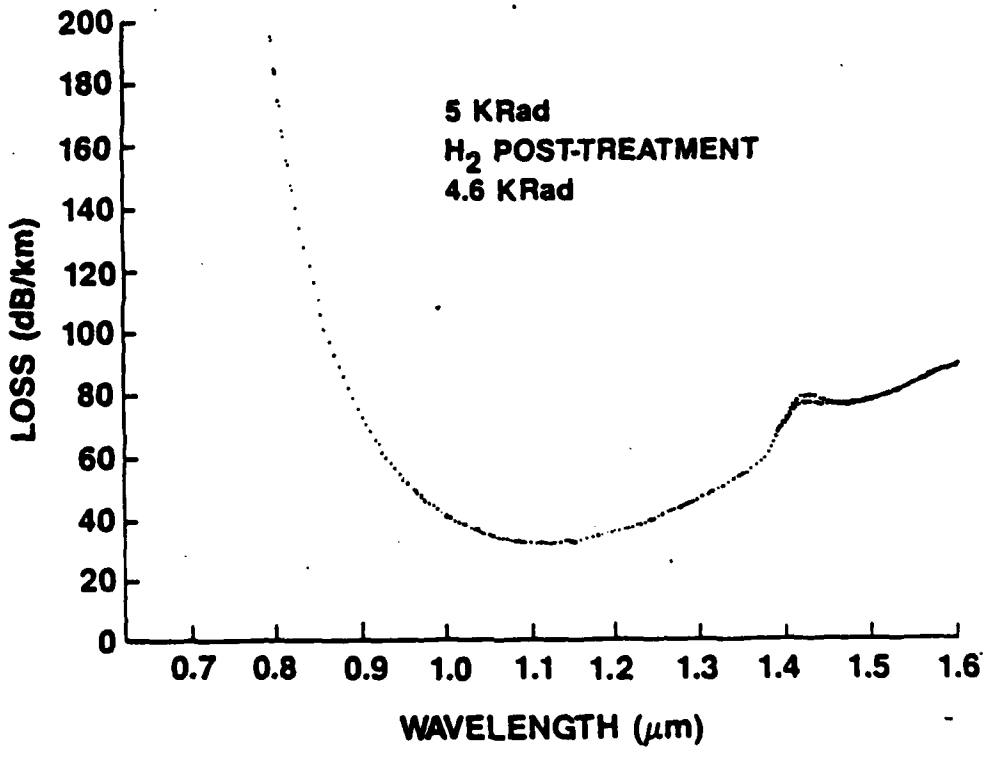

Figure 5

Loss spectra after a second 4.6 kRad dose for fibers treated with hydrogen (0.86 atm, 65°C, 7 days) following first irradiation. The upper curve is the fiber which was treated prior to the first irradiation (0.06 atm, 70°C, 7 days).

2.2 PHOTOLUMINESCENCE AND RAMAN SCATTERING

The radiation-induced loss measurements, which are the primary characterization tool used in this program, are generally not selective enough to identify the specific centers which are responsible for the absorption. In order to obtain a more selective technique for this purpose, we have explored the use of Raman scattering and photoluminescence in fibers. The objective of this line of endeavor is to identify specific color centers and precursor defects and correlate their concentrations with preform composition and fiber processing. This information, along with the knowledge of which centers are most deleterious for the transmission wavelengths of interest, will enable us to predict compositions and processing conditions which will produce fiber with the greatest radiation resistance.

Three phosphorus-doped fibers drawn from the same preform were investigated using these techniques. The samples were short sections taken from the fibers discussed in Section 2.1. These were a pristine as-drawn fiber (lower curve in Figure 1), a fiber which was irradiated without pretreatment (upper curve in Figure 4), and a fiber which was hydrogen treated and then irradiated (lower curve in Figure 4). Raman scattering was performed on these fibers using laser excitation at wavelengths ranging from 482 to 676 nm. However, it was found to be relatively insensitive to the defects of interest, and no variations could be found among the fibers or as a function of wavelength for a given fiber. Photoluminescence was found to be a very sensitive probe of defect centers and significant differences among the fibers were detected. Figure 6 compares the luminescence band at 650 nm for the three fibers before they were subjected to short wavelength (λ<530 nm) excitation. This emission band and an associated absorption band near 630 nm have been reported on by several authors who attribute it to drawing- and/or radiation-induced centers [4]. To make an absolute comparison of intensities, the emission spectra were scaled by equilizing the intensities of the Raman scattering for the different fibers. Luminescence is not detectable for the pristine fiber but is prominent for the irradiated fibers, being even more intense

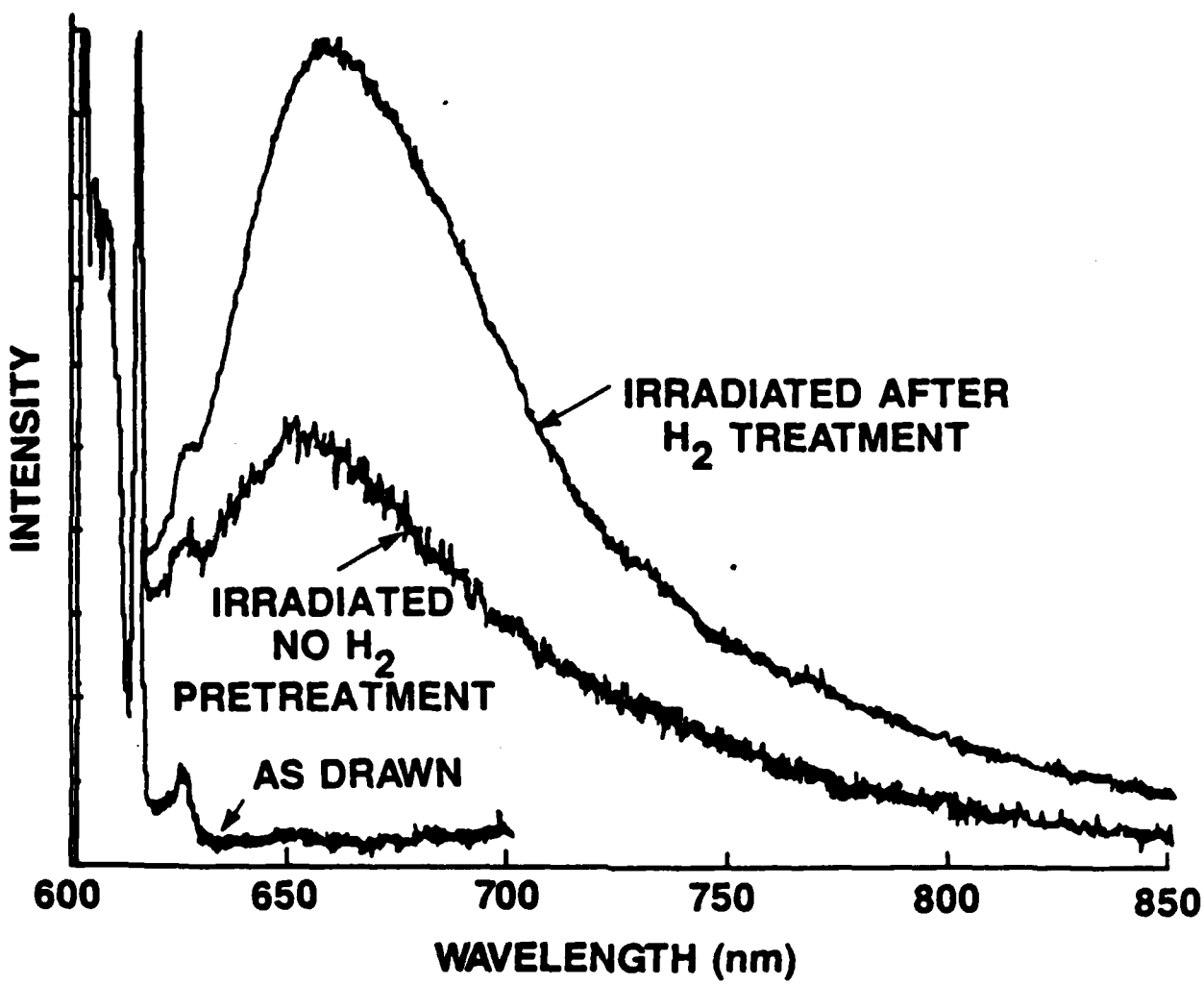

Figure 6

Comparison of luminescence intensity prior to excitation at 482 nm for fibers subjected to different treatments. The excitation wavelength was 568 nm. The sharp structure at left is Raman scattering which was used to scale the intensities for the different fibers.

for the fiber which had been hydrogen treated before irradiation. Since the latter fiber also exhibited lower losses at wavelengths >1 μm (lower curve in Figure 4), this inverse relationship to radiation-induced loss implies that this defect is not responsible for the induced long wavelength loss in these fibers. Moreover, it appears that hydrogen treatment prior to irradiation can convert defects which will result in long wavelength losses into the more benign defects which are transformed into this luminescent center when irradiated.

The photoluminescence was also found to depend upon the exciting wavelength. Figure 7 compares the emission for the three fibers when excited at 482 nm. Again, the spectra have been scaled by the Raman intensity to facilitate absolute comparisons. The fibers maintain the same hierarchy of intensities when excited at this wavelength, but the emission is considerably stronger with even the pristine fiber showing intense emission. Additional features, such as the bump at 600 nm, have appeared in the spectra and may indicate the presence of still other centers. These have not been reported in the literature and will be investigated further.

Prolonged excitation at short wavelengths (λ<530 nm) produced significant photobleaching in the irradiatied fibers which was observed through visual inspection. This occurs through photoconversion of centers which is also observed through changes in photoluminescence intensity for all three fibers. Figure 8 illustrates this phenomenon for the pristine fiber. Prior to short wavelength exposure there had been no significant emission at 650 nm when excited at 568 nm. Afterwards the luminescence band has become noticeable although still much less intense than the Raman scattering. Figure 9 shows the same effect for the fiber which had been hydrogen treated prior to irradiation. The luminescence is considerably stronger, implying an increase in concentration of this center, although the fiber loss has been significantly reduced by photobleaching.

Photoconversion of defects is a well known phenomenon in insulators and its manifestation as photobleaching has been extensively studied in fibers.

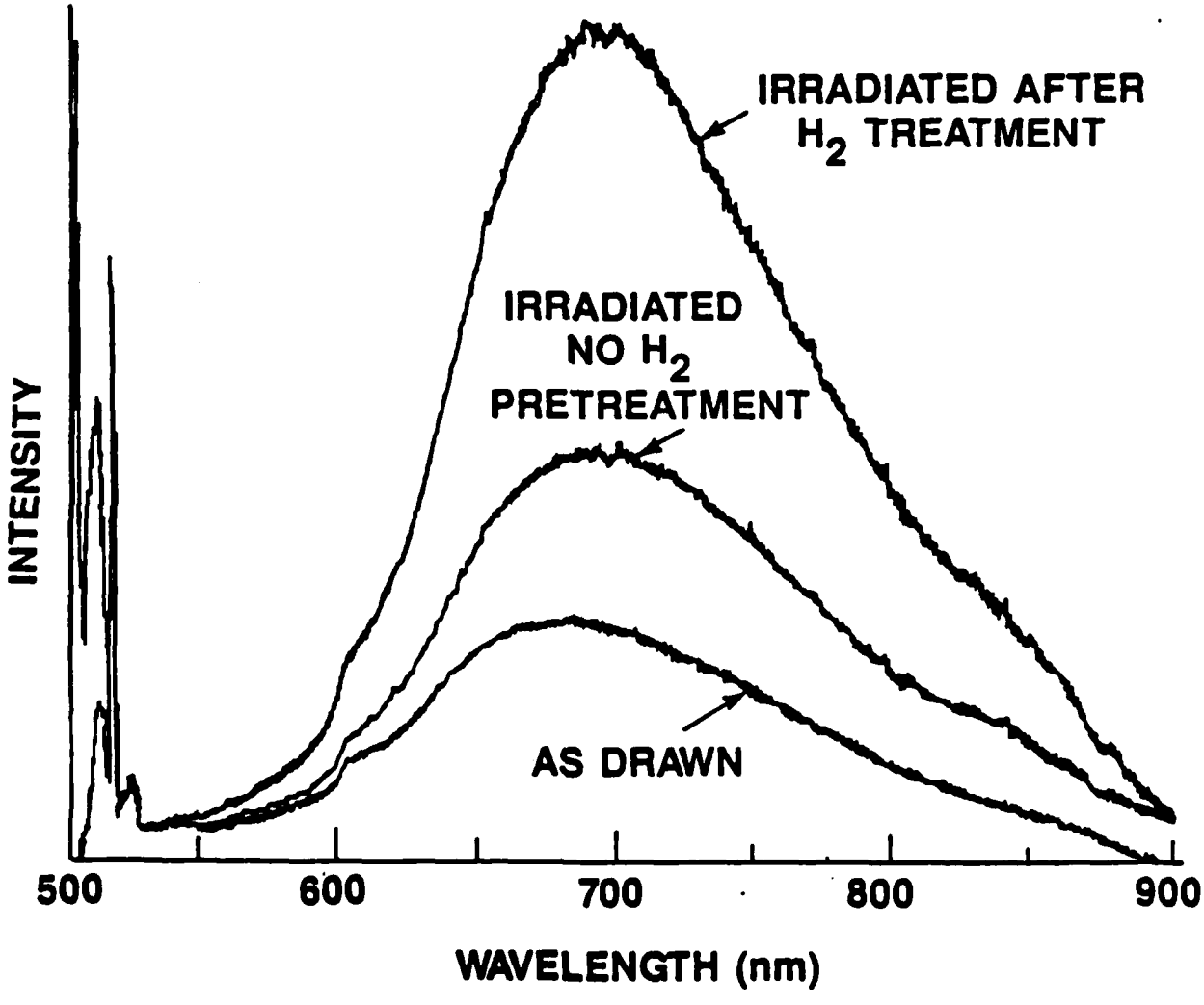

Figure 7

Comparison of luminescence intensity for fibers subjected to different treatments. The excitation wavelength was 482 nm. The sharp structure at left is Raman scattering which was used to scale the intensities for the different fibers.

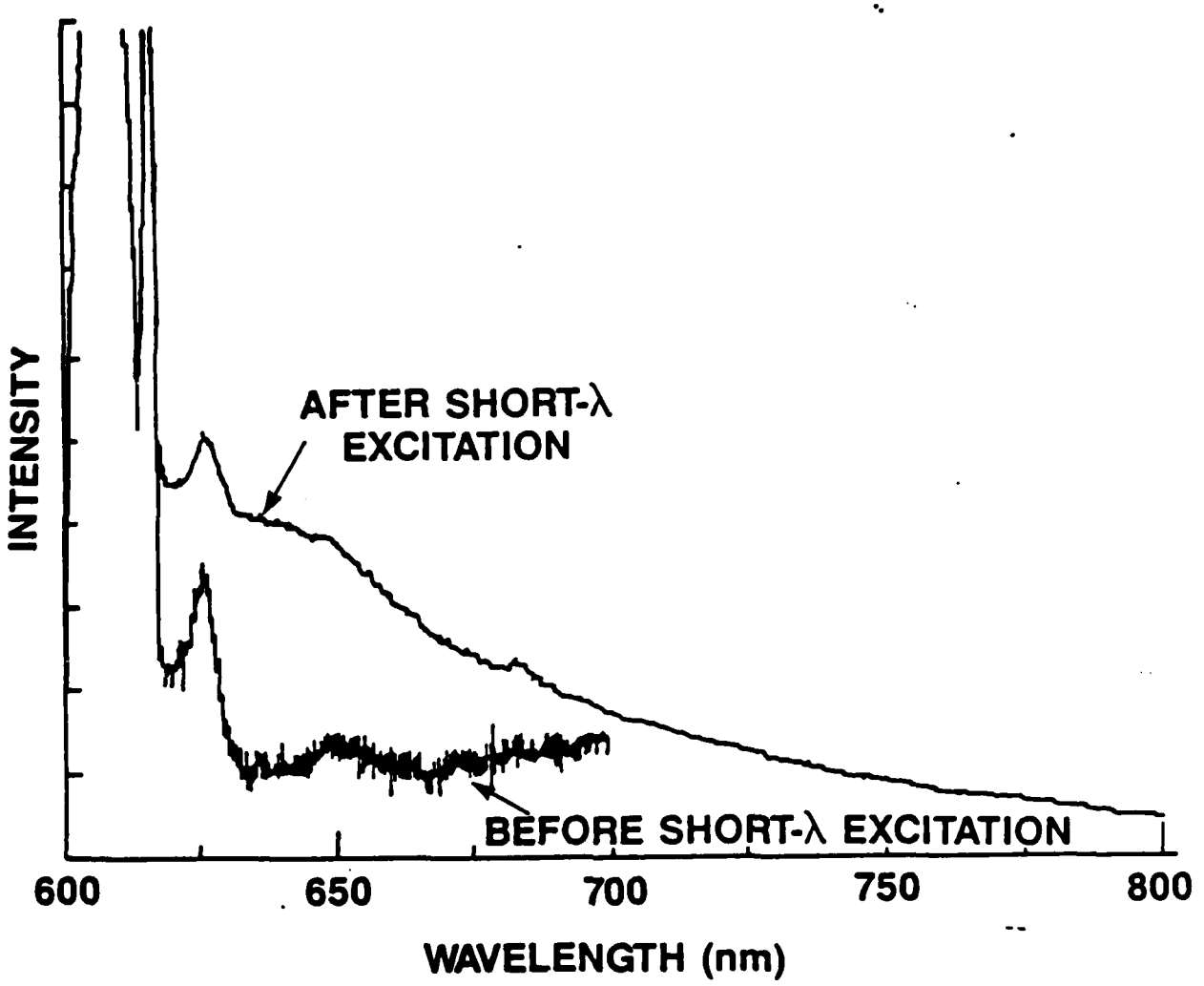

Figure 8

Comparison of luminescence intensity before and after 482-nm excitation for pristine fiber. The excitation wavelength was 568 nm. The sharp structure at left is Raman scattering which was used to scale the intensities.

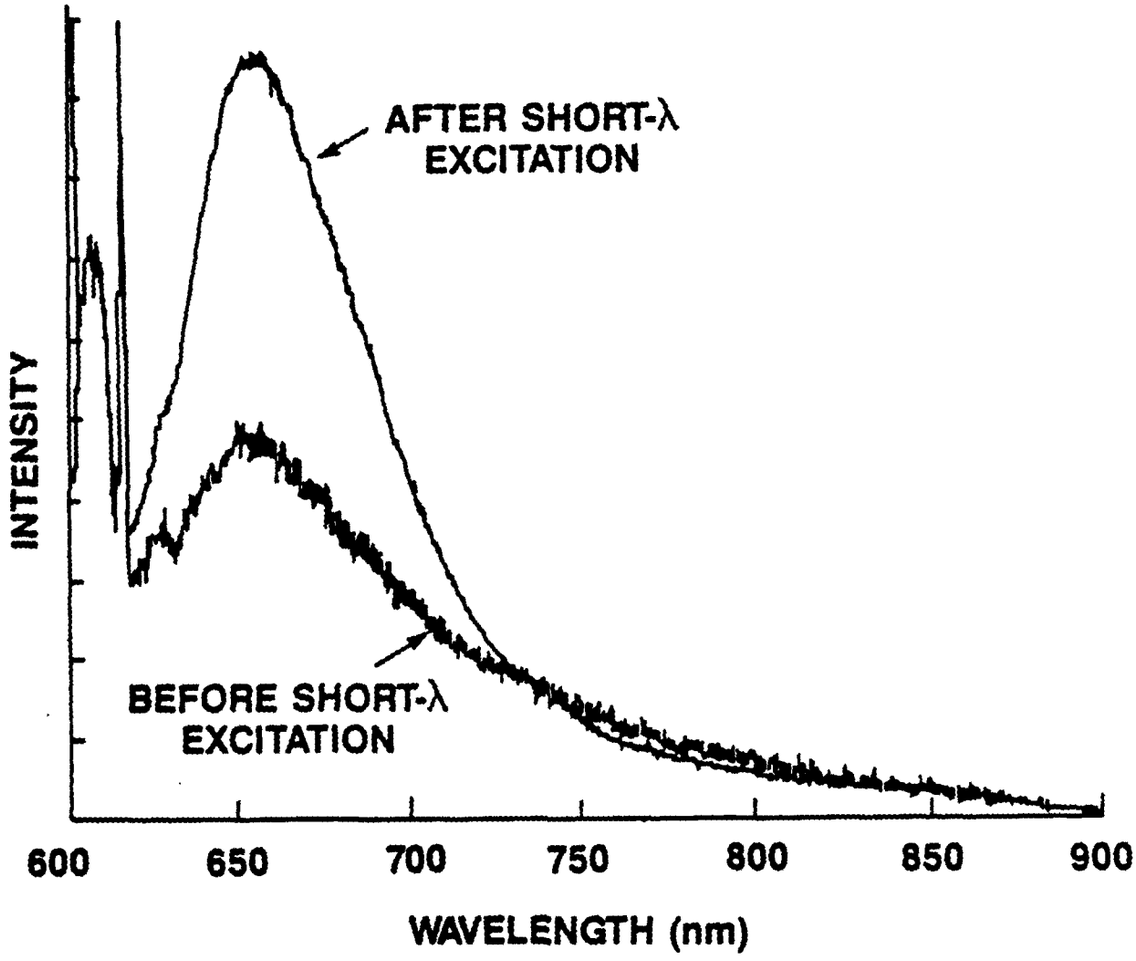

Figure 9

Comparison of luminescence intensity before and after 482-nm excitation for fiber which was treated with hydrogen prior to irradiation. The excitation wavelength was 568 nm. The sharp structure at left is Raman scattering which was used to scale the intensities.

Photoluminescence investigations such as this one will be extremely helpful in gaining new insight into types of defects present in fibers and their correlation with radiation-induced loss at long wavelengths. It has provided additional evidence for our view that radiation-induced loss can be reduced by defect conversion (passivation) before as well as after irradiation. The center responsible for the 650-nm luminescence band is an example of a relatively benign defect which can be formed by hydrogen treatment from more deleterious defects. This investigation will be extended to analyze the effects of other compositions and processing parameters.

3. DEFECT MINIMIZATION

3.1 MOLECULAR DYNAMICS SIMULATION

The molecular dynamics simulation uses computer-generated glasses to investigate the types and abundances of structural defects present in glass compositions used for fibers. The objective is to determine the effect on the defect structure of silica glass of conventional dopants as well as dopants which serve as recombination centers for the electrons and holes produced by radiation. By gaining a fundamental understanding of what types and concentrations of defects are formed by dopants, we hope to predict which dopants or combination of dopants will result in the greatest radiation hardness while providing the required refractive index modification or recombination centers.

Molecular dynamics generates the glass structure by calculating the pairwise interionic forces of a large array of ions and uses these to determine the velocity and position of the ions at a later time. The new positions are in turn used to recalculate the interionic forces. This cyclical process is repeated at short time intervals at a high temperature until the structure stabilizes. The glass is then cooled to room temperature by removing kinetic energy and suitable analysis programs are applied to examine the local structure of this computer-generated glass. Analysis programs currently available calculate the radial distribution function of each type of ion, the average diffusion rate, the velocity autocorrelation function, the distribution of neighbors, the fraction of bonds rearranged or unchanged as a function of time, and the time-dependent radial distribution function. The program used to generate the glass requires input parameters which describe the interionic forces of all

the species. In particular, repulsion parameters are required for all components; if they are not available in the literature these parameters must be chosen empirically such that interatomic distances agree with average values determined experimentally.

The computer program that generates the glass structures required partial rewriting because (1) the direct access files used by the program as it had been written and initially used were too large to retrieve from the archives with the current disk usage, and (2) the FORTRAN compiler that had been used previously had some serious problems and was replaced by a more universally compatible one. With the assistance from a systems programmer from the GTE Technical Computation Center, the program was modified to be compatible with the new compiler and use smaller files as well as run more efficiently.

The first application of the simulation program was to pure SiO_2 which was modeled as a standard to which more complex systems can be compared. The glass was initially equilibrated at 6000 K for 12-16 picoseconds (ps) and then cooled gradually to room temperature in another 16 ps. The time scale for each step in the simulation is 10^{-3} ps and each step requires ≈17 sec of CPU time on the IBM 3081. Another computer program was written to analyze the structure of the simulated glass by calculating the radial distribution function and the average coordination number as a function of distance. This program was applied to SiO_2 and the results are illustrated in Figure 10.

Studies were made to ensure that the glass was being equilibrated at 6000 K for a time sufficiently long for the structure to converge. This was done by holding the glass for longer periods of time at the high temperature before cooling to room temperature. The radial distribution function was then calculated and examined for change as a function of additional time at high temperature. This investigation revealed that about 16 ps of simulation at 6000 K followed by 16 ps of cooling to room temperature are needed to reach an equilibrated structure, i.e. one that does not change significantly with further time at 6000 K.

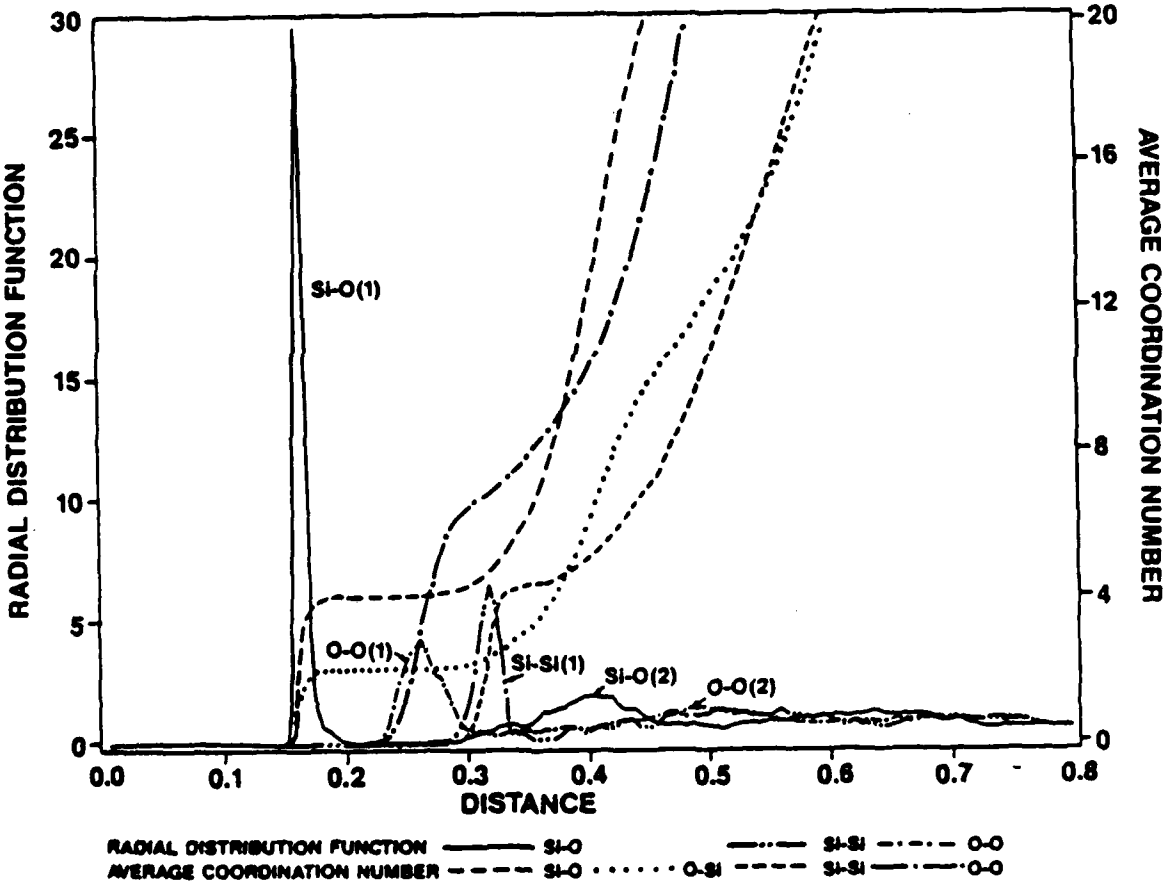

Figure 10

Radial distribution function and average coordination number as a function of distance for fused silica.

Based upon these results for SiO_2, pure GeO_2 glasses and GeO_2-doped silica glasses were generated by starting with an equilibrated SiO_2 structure, adjusting the density and therefore the box size, and allowing the structure to equilibrate for an additional 20 ps before cooling. For the Ge-containing glasses, the same parameters for oxygen were used as in the pure SiO_2 glass. The repulsive parameters for Ge were found by adjusting their values until the experimental interionic distances were obtained. The pure GeO_2 glass was simulated first in order to achieve this. The Ge-O distance in the simulated pure GeO_2 glass is 0.174 nm, the same as in x-ray diffraction studies. The Ge-Ge and O-O distances deviated by 0.01 to 0.02 nm from the expected values. These could not be adjusted without drastically changing the values for oxygen. This problem in pure GeO_2 may reflect the covalent nature of the Ge-O bond and illustrates the shortcomings of using a purely ionic potential to generate the glass structure. However, in glasses containing primarily SiO_2, the Ge-Ge interactions should be minimal and this discrepancy is not expected to have a significant effect upon the structure.

As the model system for Ge-doped silica, a glass with the composition 10 mole% GeO_2 - 90 mole% SiO_2 was generated. The simulation was done by starting with the equilibrated SiO_2 structure and replacing 6 of the 60 Si ions by Ge ions. The Ge parameters used were those obtained in the above simulation of pure GeO_2. The structure of the binary glass was then equilibrated at 6000 K for 20 ps before cooling to room temperature. To obtain a statistically valid sample, 10 cooling runs were done. Each run started with the last configuration of the previous 6000 K run and was allowed to continue for an additional 2000 steps (2 ps) at 6000 K before cooling. After cooling to 300 K and equilibrating for 1000 steps, every tenth configuration was saved so that from the ten runs, 1000 configurations could be examined. The radial distribution function, the average coordination number, and the probability that a Si ion has 3,4, or 5 oxygen ions within a certain distance were determined. Furthermore, differences between "average" Si ions and Si ions "near Ge ions" could be distinguished.

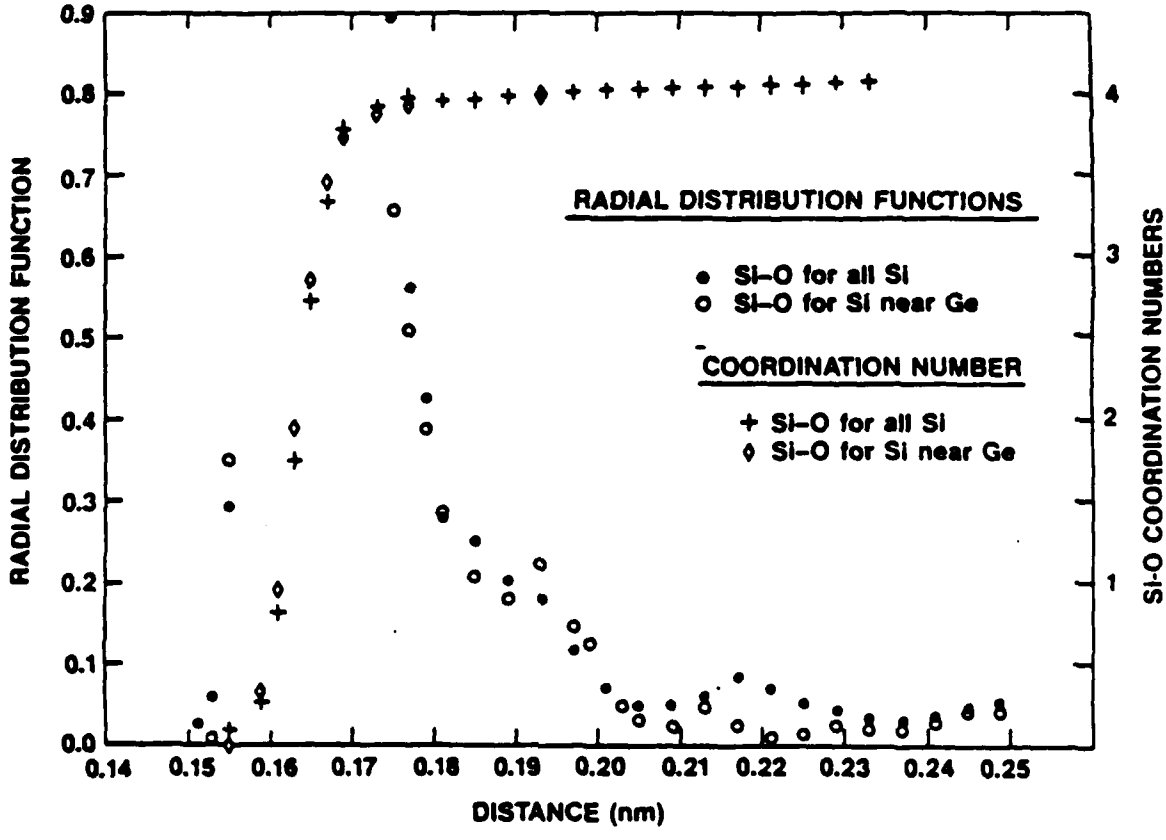

Figure 11

Radial distribution function and average coordination number as a function of distance for the 10 mole% GeO_2-doped silica glass. The vertical scale has been expanded and the peak of the rdf curve lies off scale.

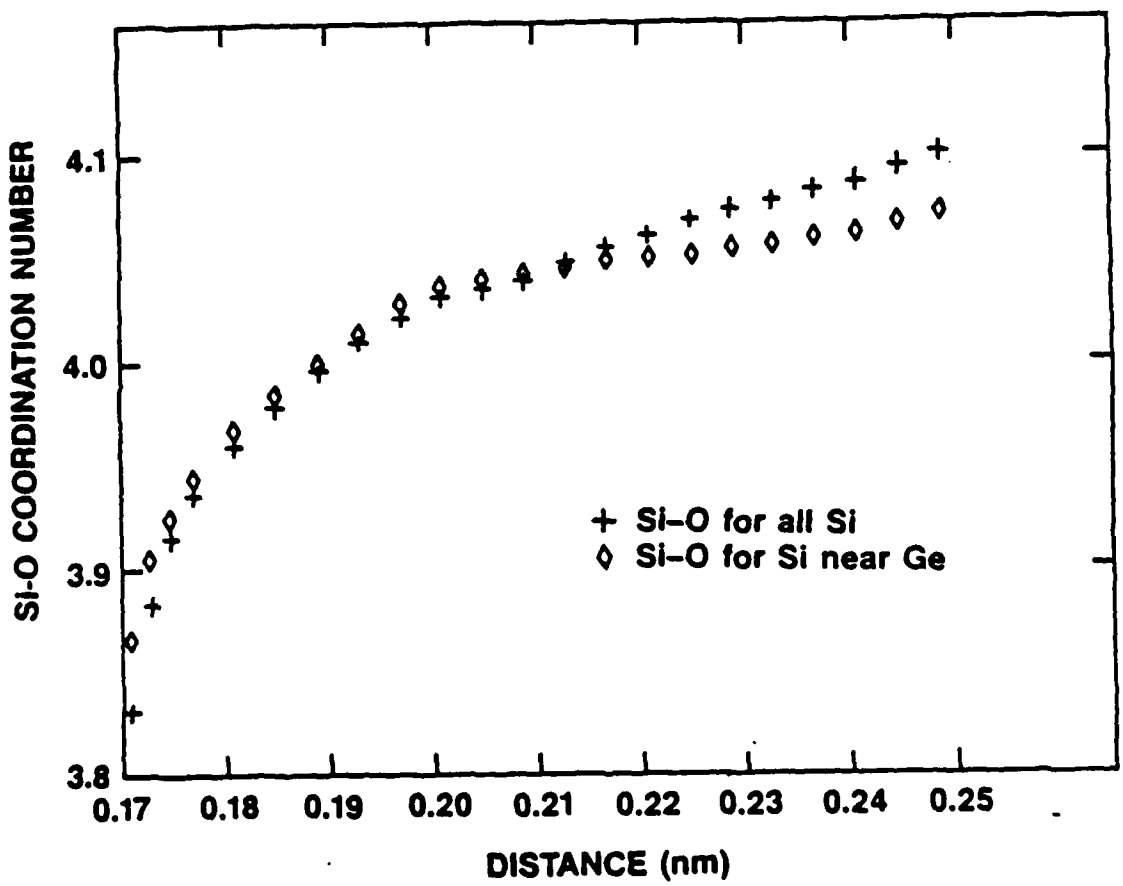

Figure 12

The average coordination number as a function of distance for the 10 mole% GeO_2-doped silica glass. The ordinate has been expanded over that of Figure 11 to illustrate the differences at distances beyond the median Si-O separation.

Examination of the coordination number at distances greater than the median Si-O distance but within the first coordination sphere shows that a number of Si ions have an oxygen coordination number greater than four. As seen in Figure 11, at distances less than 0.215 nm the oxygen coordination around Si ions near Ge ions is greater than that of "average" Si ions. At distances greater than 0.215 nm, the "average" Si ions have a larger coordination number. This can be seen clearly in Figure 12 which shows the Si-O coordination number as a function of distance on an expanded scale. The same effect is reflected in the radial distribution function (RDF). In Figure 11 only the edges of the main RDF peaks are shown, the peaks lie off-scale vertically. The nearest neighbor Si-O RDF for Si ions near Ge ions shows a "tighter" structure than for "average" Si ions. At distances greater than 0.20 nm from Si ions, the probability of finding an oxygen ion is greater for "average" Si ions than for Si ions near Ge ions. These would be the fifth oxygen surrounding a central Si ion. Thus the SiO_4 tetrahedra occasionally have an additional oxygen ion crowding them. Another way of looking at these results is that the coordination number of Si ions near Ge ions is closer to four than that of "average" Si ions because of the narrower distribution in distances to oxygens. This is also represented in the probability that Si ions will have an oxygen coordination number of five as shown in Table 1. The effect is particularly noticeable at distances of 0.215-0.24 nm from Si ions.

Thus far this analysis indicates that defects, in terms of stretched Si-O bonds near Ge, are not observed in this glass. Defects produced by Ge doping which are susceptible to radiation must be of another type. They could be found in Ge-O bonds themselves or in "average" Si-O bonds which differ from those in pure SiO_2. From x-ray studies of pure GeO_2, it has been found that there is a very narrow distribution of Ge-O-Ge intertetrahedral angles and the randomness in the glass structure is attributed to tetrahedra twisting. Whether this can be extended to SiO_2-GeO_2 glass has yet to be determined. If this is the case, then constraints may be placed on the network which are not seen in pure SiO_2. The defect structure would then be more

TABLE 1

PROBABILITY OF Si HAVING N OXYGEN NEIGHBORS AS A FUNCTION OF NEIGHBOR DISTANCE D

A. All Si Ions

N	PROBABILITY		
	0.146 < D < 0.186 (nm)	0.146 < D < 0.215 (nm)	0.146 < D < 0.240 (nm)
3	0.024	0	0
4	0.973	0.952	0.916
5	0.003	0.048	0.084

B. Si Ions With a Ge Neighbor at Distance Within Range 0.25–0.4 nm

N	PROBABILITY		
	0.146 < D < 0.186 (nm)	0.146 < D < 0.215 (nm)	0.146 < D < 0.240 (nm)
3	0.018	0	0
4	0.979	0.933	0.939
5	0.003	0.047	0.061

complicated than just abnormal ionic distances and might include ring structures.

Detailed structural analysis of this type will also be performed on pure SiO_2 and GeO_2 glasses. Comparison of those results to the ones presented here for the doped glass will assist us in determining the types of defects generated when silica and germania are mixed. This analysis is in progress.

To continue the molecular dynamics study of optical fiber glasses, a SiO_2-GeO_2-F glass is being simulated. The repulsive parameter being used for fluorine is that of Tosi and Fumi for fluoride salts [5]. The initial structure is that of an equilibrated SiO_2-GeO_2 glass with the appropriate substitutions, and the structure is being allowed to equilibrate for 20 ps at 6000 K before cooling.

3.2 DRAWING INDUCED DEFECTS

In this aspect of the program the influence of drawing conditions on the radiation sensitivity of fiber is investigated. Four fibers were drawn from the same preform at extremes of the interdependent parameters of temperature, speed, and tension. Examination of the loss spectra before and after irradiation will indicate the role of the fiber drawing process in generating defects which become color centers.

A graded index preform was fabricated for this investigation of drawing-induced defects. The preform had a constant fluorine doping level across both clad and core and a Ge doped core. Four 800-m sections of optical fiber were drawn under the four different sets of drawing conditions listed in Table 2. The furnace temperature and draw speed were selected to intentionally vary the induced defect concentration among the fibers. Figures 13-16 illustrate the loss spectra of these fibers measured from 600-1600 nm before and after a γ radiation dose of $\approx$20 kRad. The oscillatory structures in Figures 14 and 16 are probably due to weak guiding resulting from the depressed inner clad. We intend to study in greater detail the differences in fiber attenuation prior to irradiation and their relationship to drawing-induced defects using additional techniques such as Raman scattering and photoluminescence.

Table 2 also summarizes the loss results at 850 nm before and after irradiation. The fibers drawn at the lower furnace temperature showed an over-

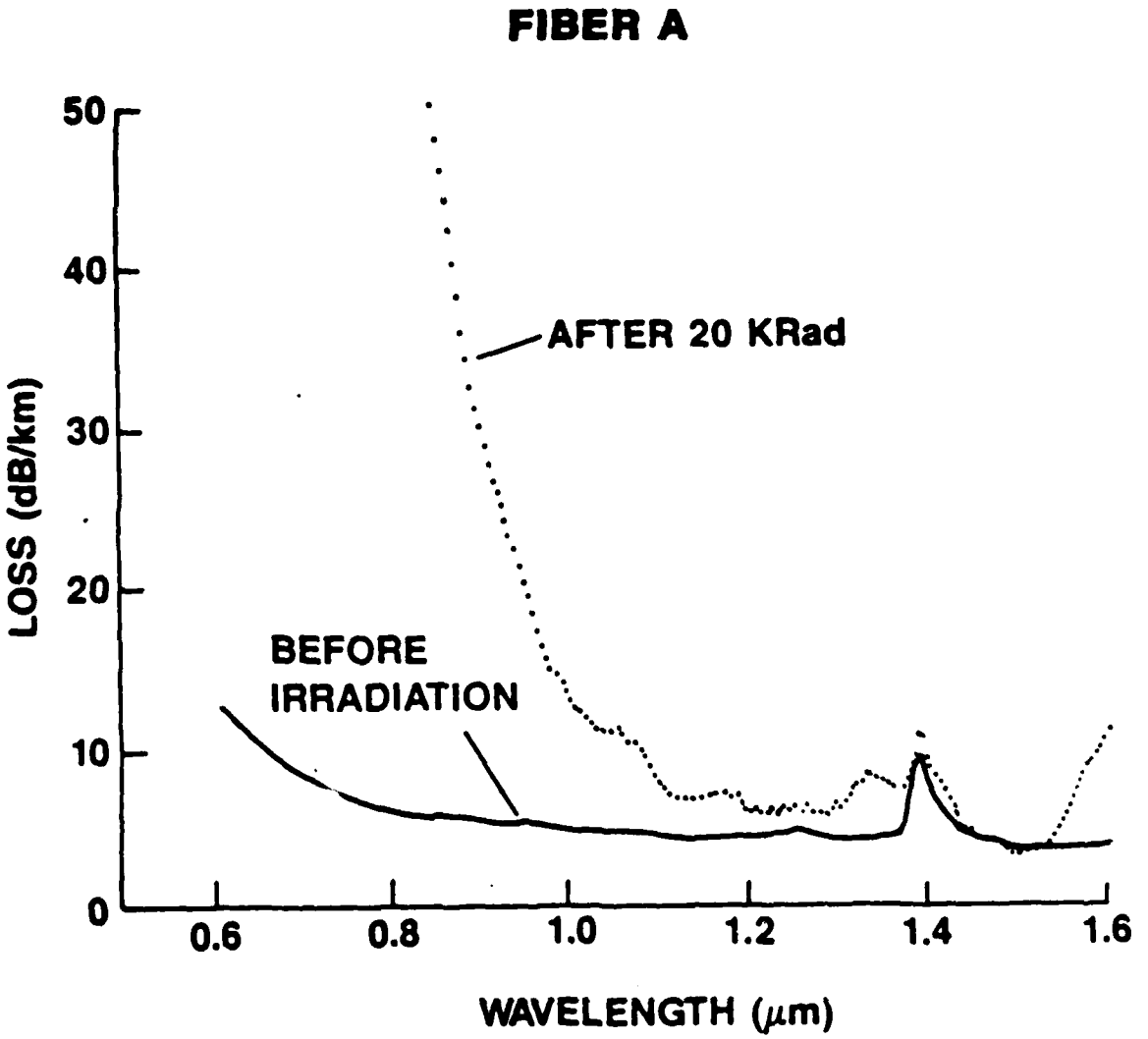

Figure 13

Loss spectrum of fiber A before and after 21 kRad irradiation.

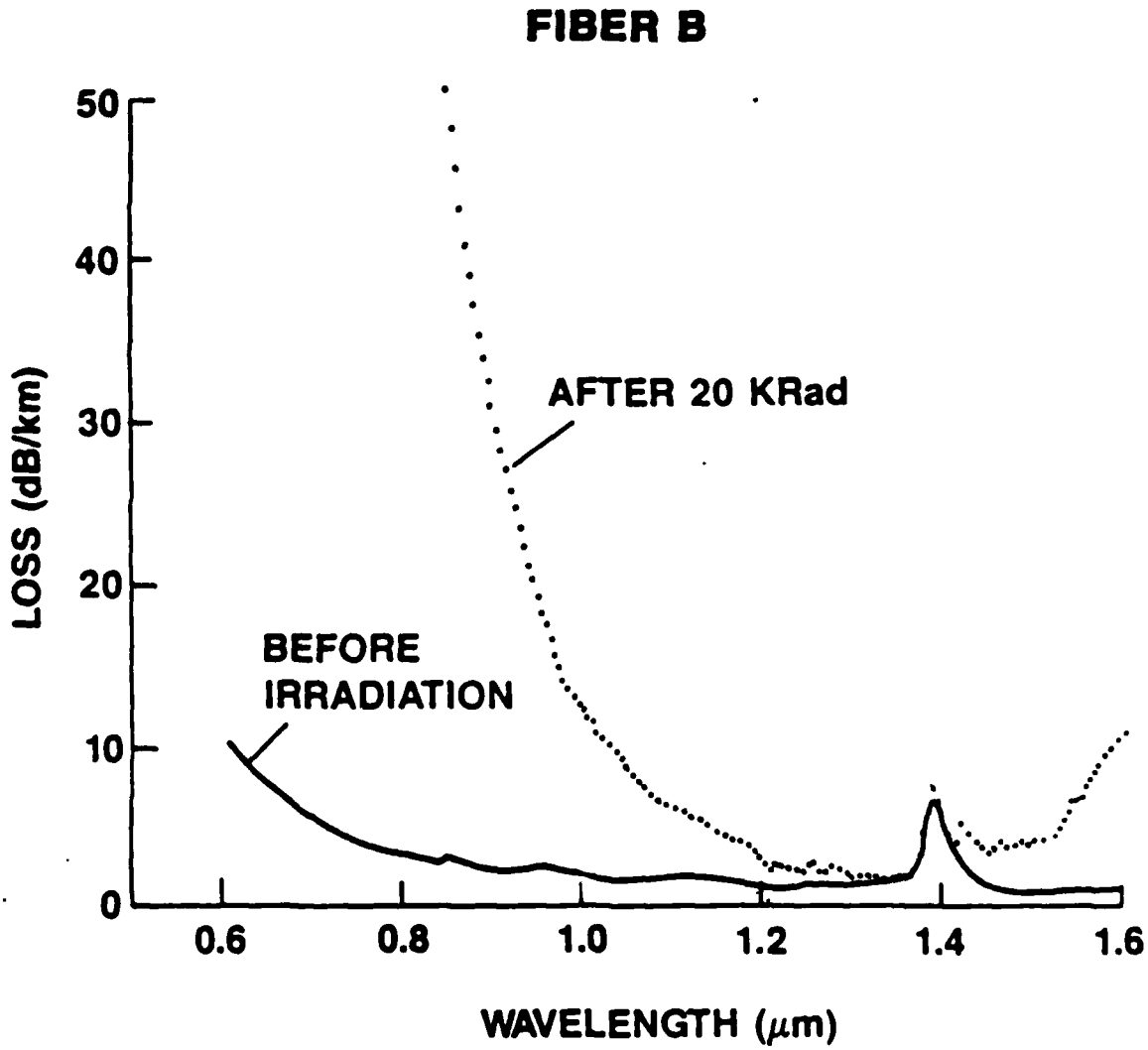

Figure 14

Loss spectrum of fiber B before and after 22 kRad irradiation.

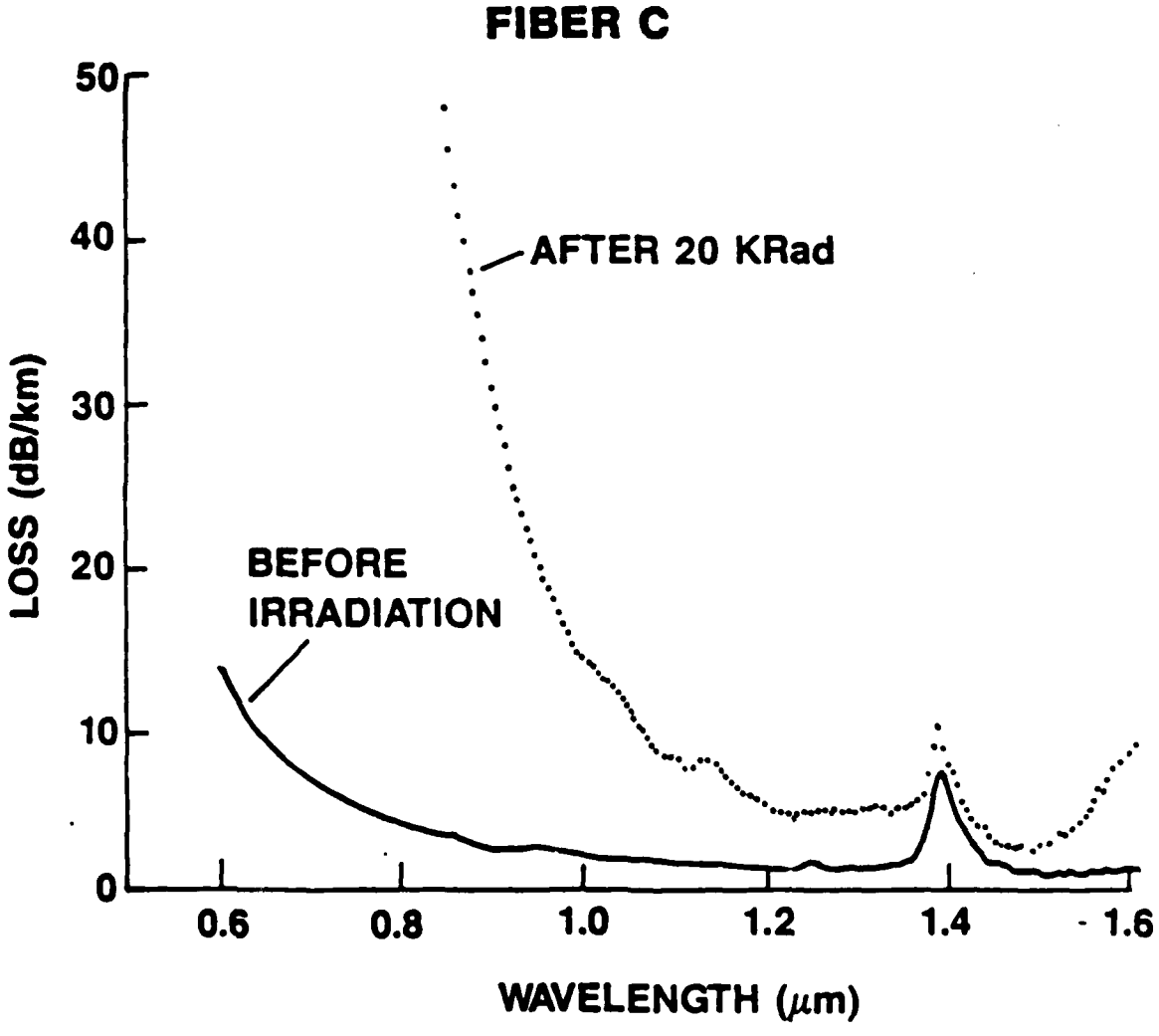

Figure 15

Loss spectrum of fiber C before and after 22 kRad irradiation.

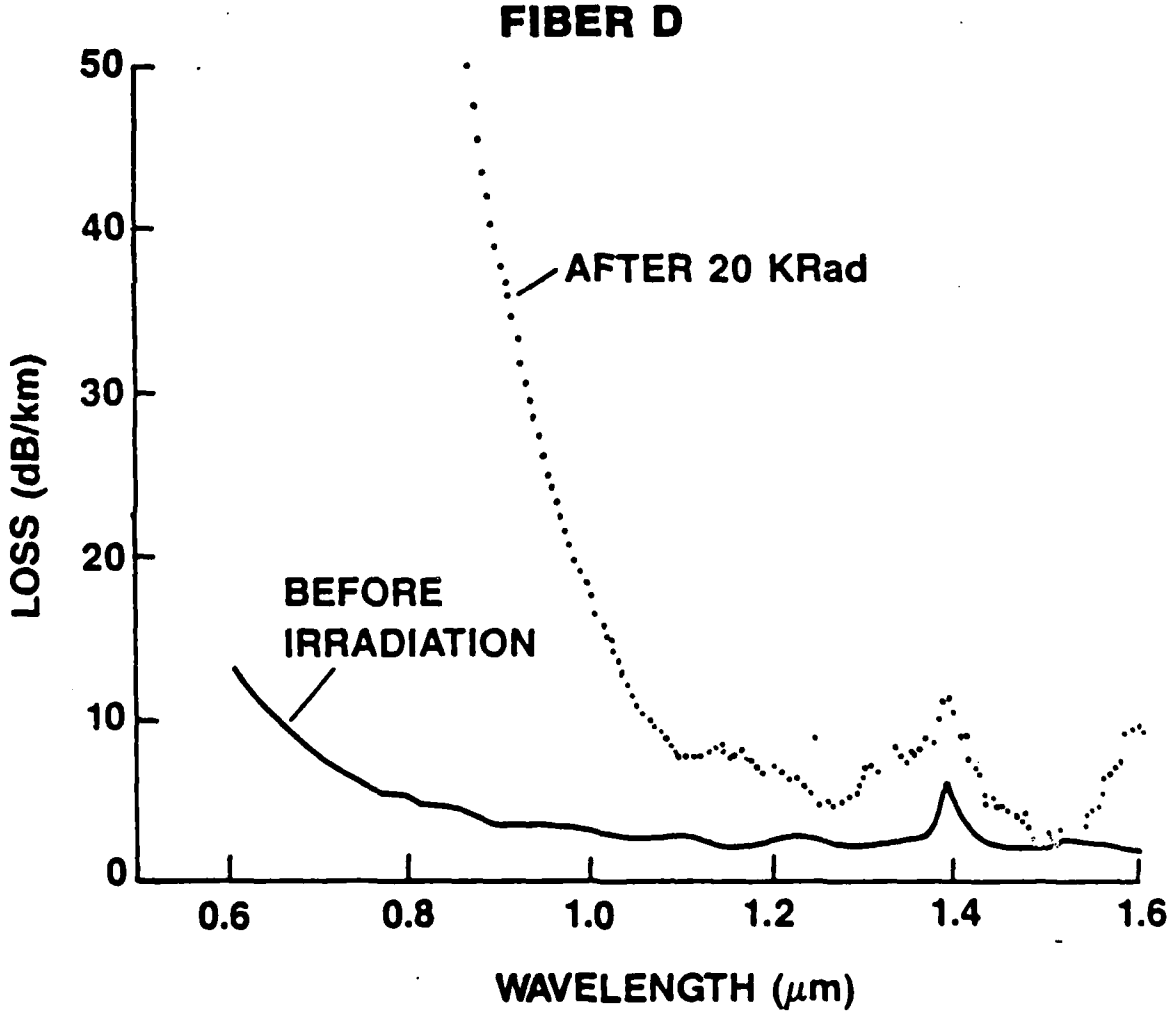

Figure 16
Loss spectrum of fiber D before and after 24 kRad irradiation.

TABLE 2

SUMMARY OF RESULTS FOR THE INVESTIGATION OF THE EFFECT OF DRAWING PARAMETERS ON RADIATION-INDUCED LOSS

Fiber Designation	Draw Parameters			Loss at 850 nm (dB/km)				
	Temperature (°C)	Speed (m/s)	Tension (g)	Before Irradiation	After Irradiation	Induced Loss (GTE Labs)	Induced Loss (RADC)	Loss/KRad
A	1825	0.5	25	5.3	45.6	40.3	35	1.68
B	1825	1.0	50	2.3	47.6	45.3	41	1.86
C	1880	0.5	13-14	2.8	44.8	42.0	42	1.89
D	1880	1.0	~25	3.6	52.2	48.6	45	1.86

all lower radiation-induced loss, especially at longer wavelengths (≈1.3 μm). The loss values at 850 nm agreed with *in situ* results obtained at RADC shown in Figure 17. It is generally believed that fiber drawn at a lower temperature has a lower fictive temperature and, consequently, a lower defect concentration. This is in agreement with our experimental results. The effect of draw speed is less clear and further study will be necessary in order to understand it. The results of this investigation, specifically the advantages of fluorine doping in the core and the use of lower draw temperatures, are also being applied to subsequent work in the other approaches.

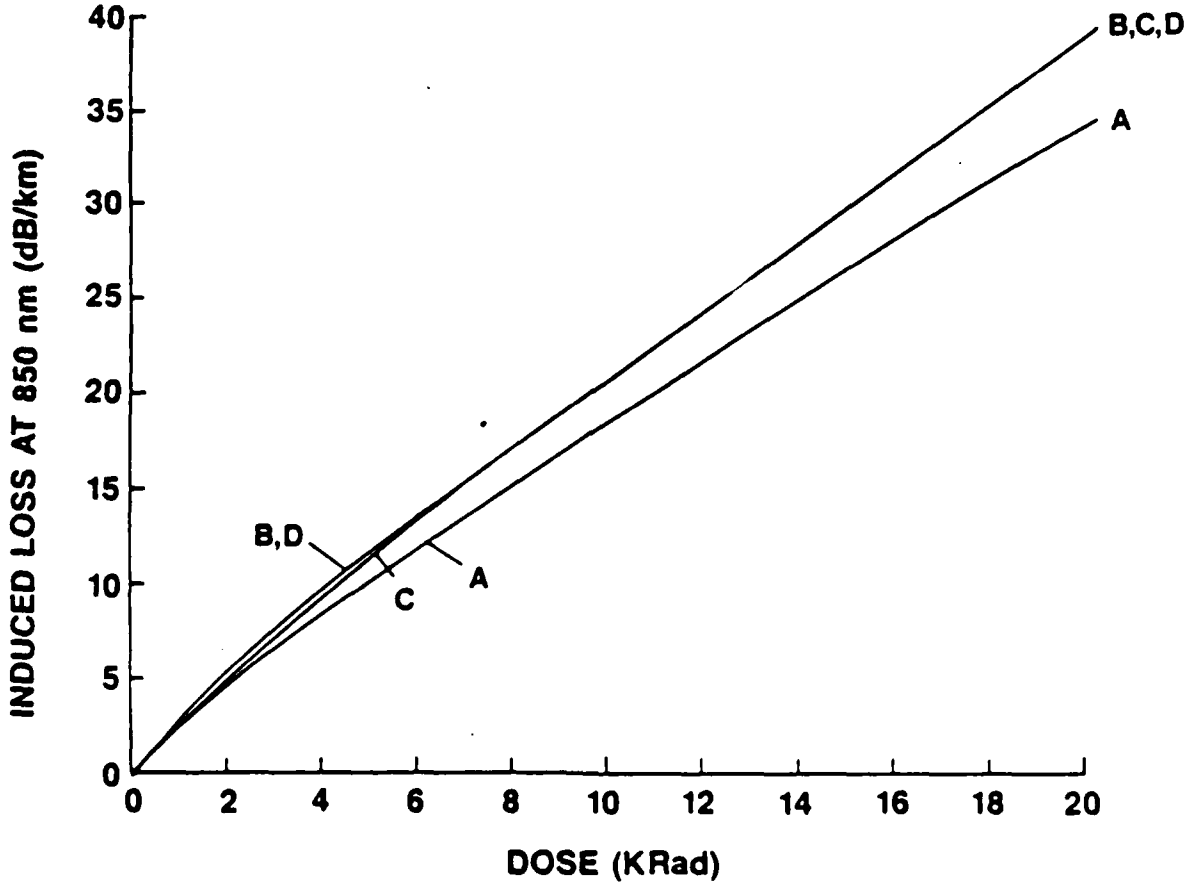

Figure 17

The induced loss at 850 nm as a function of γ radiation dose measured *in situ* for the fibers used to evaluate the role of drawing parameters.

3.3 STRESS-INDUCED DEFECTS

Thermomechanical stresses arise in optical fibers because of the different thermal characteristics of the glasses used for the core and the cladding. In general, this produces a tensile stress in the more heavily doped core causing atomic bonds to lengthen and possibly rupture, thereby creating defects. This study is intended to assess the impact of thermomechanical stress on radiation hardness and identify ways to reduce the number of stress-induced defects.

To examine the effect of core/clad interfacial stress on defect concentrations, we prepared two preforms with different clad compositions which also kept the index profile the same. The first one, having a pure silica clad and GeO_2/F codoped core, provides a high core/clad interfacial stress due to differences in thermal expansion and glass transition temperatures. The second one, having a GeO_2/F codoped clad and GeO_2/F codoped graded-index core, minimizes the core/clad stress. In both preforms the fluorine doping was maintained at a constant level and the index of the clad was matched to that of the substrate tube. Electron microprobe results verify that the desired structure was achieved and reveal high concentration gradients for both Ge and F across the core/clad interface in the first preform, in contrast to slowly varying profiles for the second preform. We have drawn both preforms into fibers using optimized draw parameters as determined by the results of the above investigation of drawing-induced defects (Section 3.2). Two draw speeds were used for each preform.

Table 3 summarizes results for the investigation of the effect of stress reduction on radiation-induced loss. Fibers designated HA and HB were drawn from the preform with a high core/clad interfacial stress, while fibers LA and LB were from a low stress preform. All these fibers show excellent radiation resistance. The induced losses at both 850 nm and 1300 nm are quite low compared to fibers with only GeO_2 doped cores. Figures 18 to 21 compare loss spectra of these fibers before and after a dose of ≈20 kRad. To

TABLE 3

SUMMARY OF RESULTS FOR THE INVESTIGATION OF THE EFFECT OF STRESS REDUCTION ON RADIATION-INDUCED LOSS

Fiber Designation	Draw Speed (m/s)	Loss at 850 nm (dB/km)			Loss at 1300 nm (dB/km)		
		Before Irradiation	After Irradiation	Induced Loss	Before Irradiation	After Irradiation	Induced Loss
HA	0.5	2.43	34.2	31.8	0.80	1.46	0.66
HB	1.0	2.63	34.0	31.4	0.92	3.84	2.92
LA	0.5	2.42	33.2	30.8	0.84	3.14	2.30
LB	1.0	2.58	29.9	27.3	0.92	2.38	1.46

further clarify the stress effect, we used the differential modal attenuation (DMA) technique to monitor the attenuation of a specific group of modes. Figures 22 and 23 show DMA results at 1300 nm for fibers drawn from preforms having high and low stress, respectively. In general, DMA data demonstrate higher losses for higher modes. The DMA measurements do not correlate well with the attenuation measurements, however, since mode filters were used for the latter. Mode filters remove the higher modes, and thus the loss results only reflect attenuation of lower modes. Before irradiation, the stress causes a steady increase in attenuation with increasing mode number (Figure 22). For a low stress fiber (Figure 23) the increase is slight and gradual. After irradiation, we do not observe any significant difference between fibers with different stresses in attenuation and DMA data.

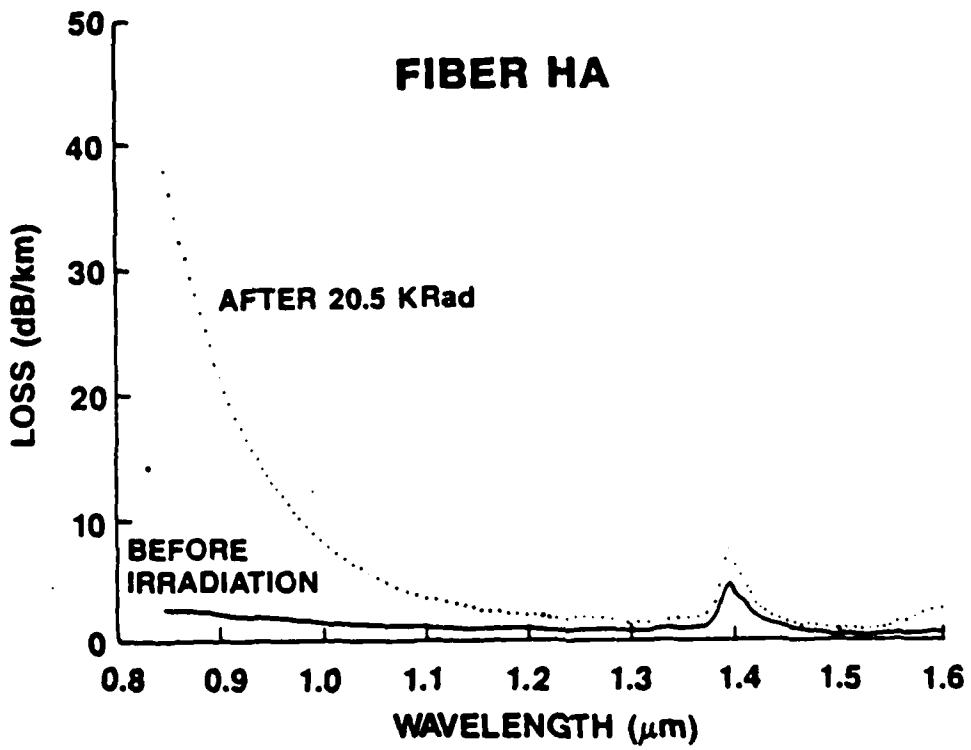

Figure 18

Loss spectrum of high stress fiber HA before and after 20.4 kRad irradiation.

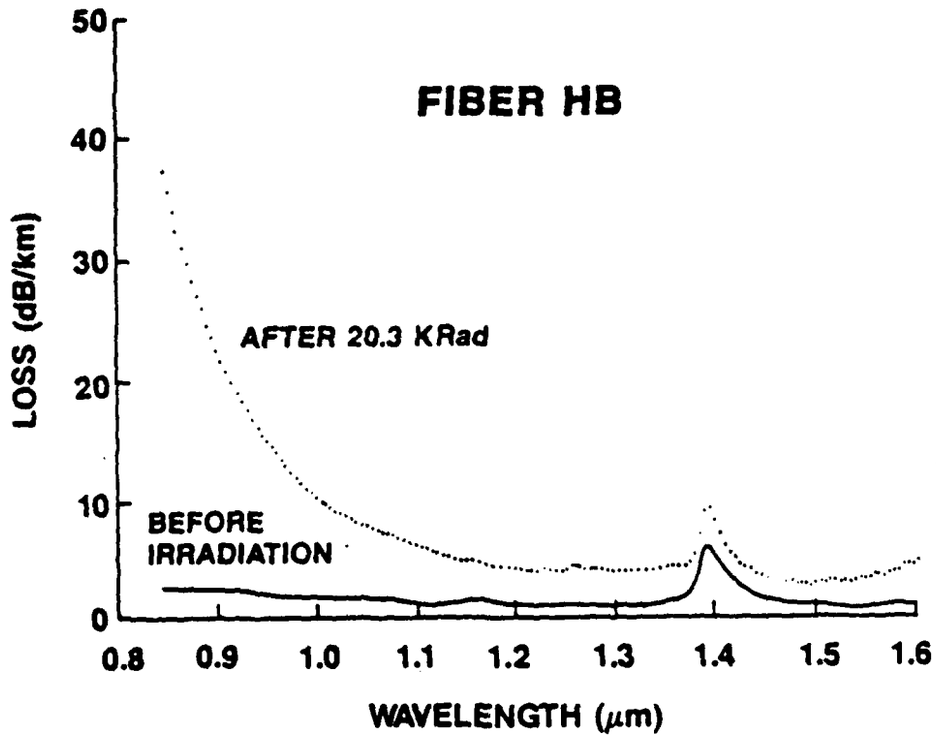

Figure 19

Loss spectrum of high stress fiber HB before and after 21.1 kRad irradiation.

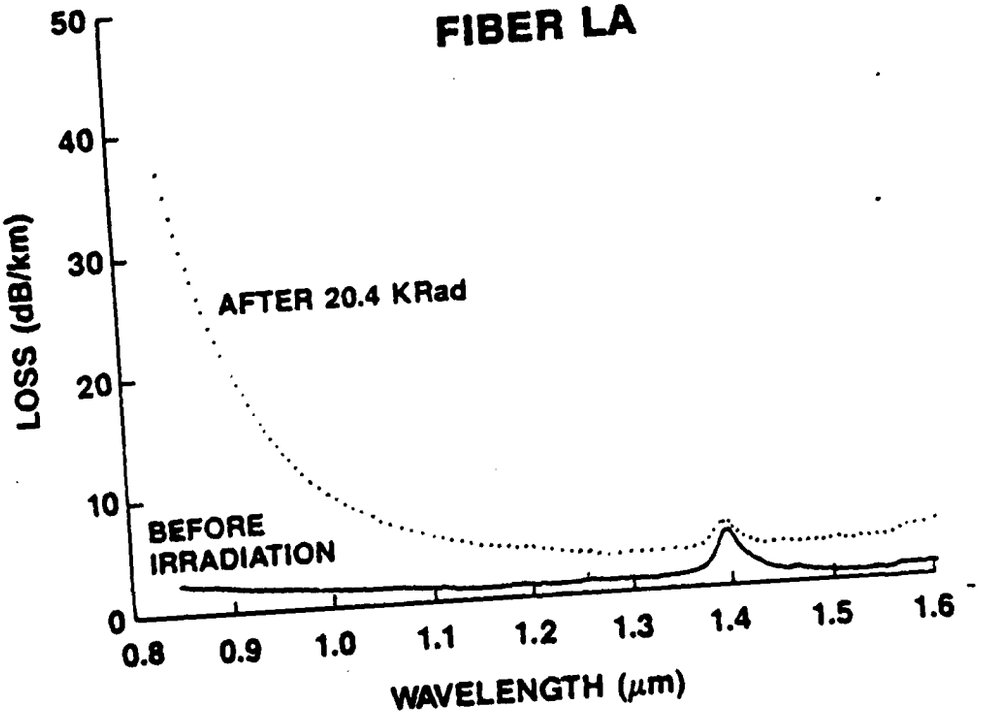

Figure 20

Loss spectrum of low stress fiber LA before and after 20.5 kRad irradiation.

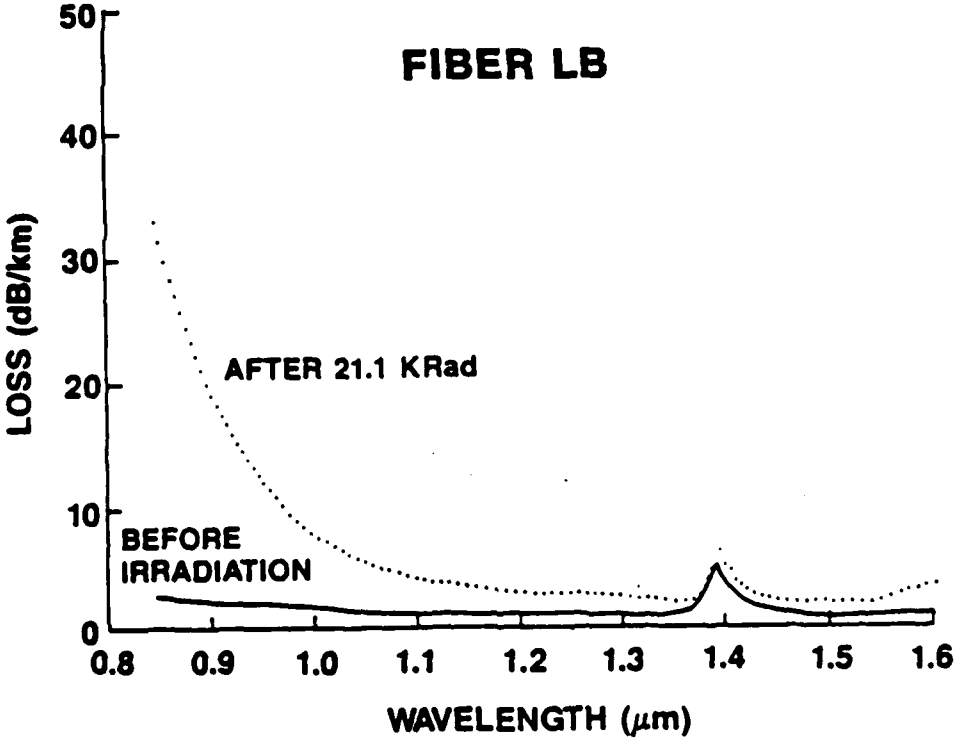

Figure 21

Loss spectrum of low stress fiber LB before and after 20.3 kRad irradiation.

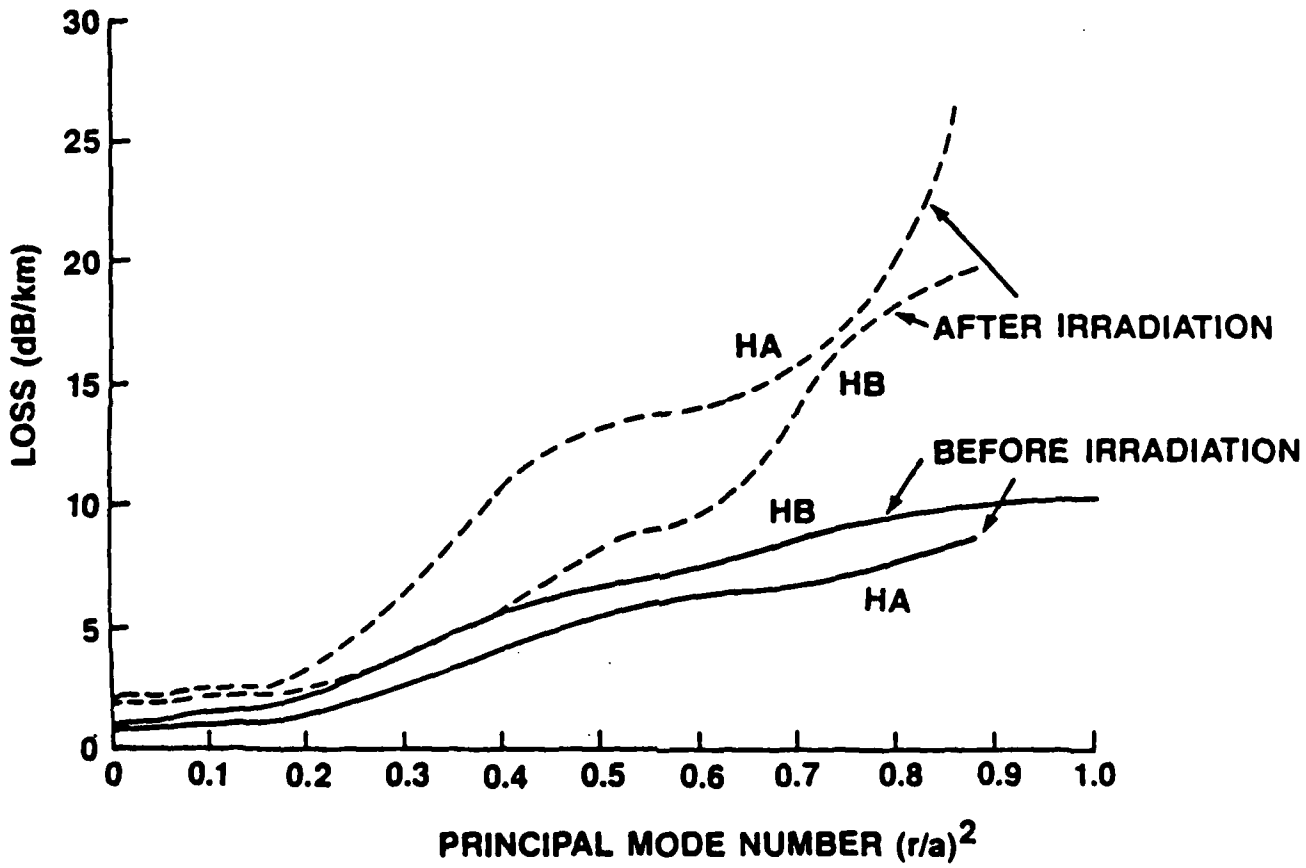

Figure 22

DMA results before and after irradiation of fibers with high stress.

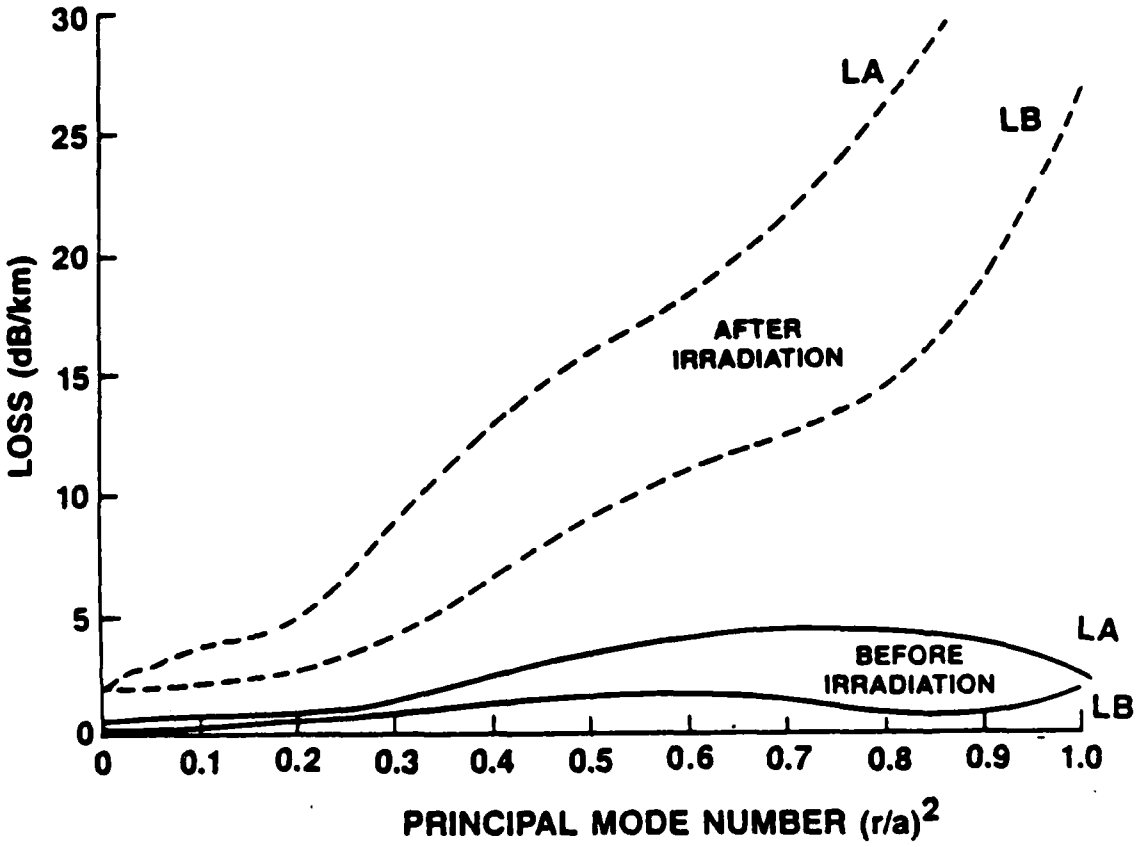

Figure 23

DMA results before and after irradiation of fibers with low stress.

Prior to this investigation, there was no known information on the spatial distribution of radiation-sensitive defects produced by core/clad interfacial stress. These results suggest that these stresses introduce defects only near the interface, resulting in higher attenuation for higher modes. Since the higher modes do not propagate a great distance in a fiber, however, stress reduction does not contribute materially to radiation hardness. Moreover, the absence of significant differences in the attenuation of the higher modes following irradiation implies that the defects produced by stress either are not great in number or are not very sensitive to γ radiation.

3.4 DOPANT REDUCTION

Dopants influence the concentration of defects in as-drawn fibers, as they do in bulk glass, by altering the glass structure. To evaluate the effect of dopant reduction on radiation resistance, we have fabricated three preforms with different Ge and F dopant concentrations in the core. These preforms have concentration ratios of 1/0.86/0.73 for germanium and 1/0.5/0 for fluorine. The reduction was introduced in such a way as to preserve the index profile and minimize the core/clad stress. Fibers drawn from this series of preforms will be irradiated at the RADC γ source and fully characterized.

4. REFERENCES

[1] J. Acocella, M. Takata, M. Tomozawa, and E.B. Watson, J. Amer. Cer. Soc. *64*, C-83 (1981); J. Acocella, M. Takata, M. Tomozawa, E.B. Watson, and J.T. Warden, J. Amer. Cer. Soc. *65*, 407 (1982).

[2] E.J. Friebele, G.H. Sigel, Jr., and M.E. Gingerich, in *Fiber Optics: Advances in Research and Development*, p. 335, B. Bendow and S.S. Mitra, eds., Plenum, NY (1979).

[3] For example, N. Uchida *et al.*, in *Proceeding 9th European Conference on Optical Communications*, p. 525 (1983).

[4] M.J. Marrone, Appl. Phys. Lett. *38*, 115 (1981); W. Carvalho, P. Dumas, J. Corset, and V. Neumann, in *Proceedings of Optical Fibers in Adverse Environments*, SPIE Vol. *404*, p. 76 (1983); E.J. Friebele, D.L. Griscom, and M.J. Marrone, J. Non-Cryst. Solids *71*, 133 (1985); and references therein.

[5] M.P. Tosi and F.G. Fumi, J. Phys. Chem. Solids *25*, 45 (1964).

MISSION
of
Rome Air Development Center

RADC plans and executes research, development, test and selected acquisition programs in support of Command, Control, Communications and Intelligence (C^3I) activities. Technical and engineering support within areas of competence is provided to ESD Program Offices (POs) and other ESD elements to perform effective acquisition of C^3I systems. The areas of technical competence include communications, command and control, battle management, information processing, surveillance sensors, intelligence data collection and handling, solid state sciences, electromagnetics, and propagation, and electronic, maintainability, and compatibility.

END

4-87

DTIC